REPORT DOCUMENTATION PAGE

Form Approved
OMB No. 0704-0188

1. AGENCY USE ONLY (Leave blank)	2. REPORT DATE	3. REPORT TYPE AND DATES COVERED
	20 Oct 95	

4. TITLE AND SUBTITLE Turbulent Kinetic Energy Budgets from a Large-Eddy Simulation of Airflow Above and within a Forest Canopy

5. FUNDING NUMBERS

6. AUTHOR(S)

Michael John Dwyer

7. PERFORMING ORGANIZATION NAME(S) AND ADDRESS(ES)

AFIT Students Attending:

University of California

8. PERFORMING ORGANIZATION REPORT NUMBER

95-124

9. SPONSORING/MONITORING AGENCY NAME(S) AND ADDRESS(ES)

DEPARTMENT OF THE AIR FORCE
AFIT/CI
2950 P STREET, BLDG 125
WRIGHT-PATTERSON AFB OH 45433-7765

10. SPONSORING/MONITORING AGENCY REPORT NUMBER

11. SUPPLEMENTARY NOTES

12a. DISTRIBUTION/AVAILABILITY STATEMENT

Approved for Public Release IAW AFR 190-1
Distribution Unlimited
BRIAN D. Gauthier, MSgt, USAF
Chief Administration

12b. DISTRIBUTION CODE

13. ABSTRACT *(Maximum 200 words)*

19951031 109

14. SUBJECT TERMS			15. NUMBER OF PAGES 77
			16. PRICE CODE
17. SECURITY CLASSIFICATION OF REPORT	18. SECURITY CLASSIFICATION OF THIS PAGE	19. SECURITY CLASSIFICATION OF ABSTRACT	20. LIMITATION OF ABSTRACT

Turbulent Kinetic Energy Budgets from a Large-Eddy Simulation of Airflow Above and Within a Forest Canopy

by

Michael John Dwyer
B.S. (University of California, Davis) 1987

THESIS

Submitted in partial satisfaction of the requirements for the degree of

MASTER OF SCIENCE

in

Atmospheric Science

in the

GRADUATE DIVISION

of the

UNIVERSITY OF CALIFORNIA

DAVIS

Approved:

Committee in Charge

1995

ACKNOWLEDGMENTS

I thank my advisor Dr. Roger H. Shaw whose guidance led to the successful completion of this thesis. His professional and personal example motivate his students to excel. I have benefited both academically and personally due to my association with Dr. Shaw.

In addition, I am grateful to my other committee members, Drs. Kyaw Tha Paw U and John J. Carroll. Both provided invaluable suggestions that resulted in several improvements to the final version of this thesis. Dr. Terry Nathan also provided very stimulating conversations that helped improve this thesis.

Several of my fellow students were instrumental in the successful completion of my studies at UC Davis. Ned Patton was a great help with many aspects of coding and data analysis. Thanks Ned. I extend a special thanks to Donna Charlevoix, Eugene Cordero, and Chris Pagliccia for being wonderful friends during my time at UC Davis.

I thank the US Air Force for my selection to attend UC Davis under the AFIT/CI program. Finally, and most importantly, none of this work would have been possible without the generous support provided by the National Science Foundation under grant No. ATM-9216345.

ABSTRACT

Large-eddy simulation (LES) output was used to study the terms of the resolved scale turbulent kinetic energy budget (TKE). The computation produces a three-dimensional, time dependent simulation of the airflow above and within a plant canopy where the lowest third of the domain was occupied by a drag layer and heat sources that represented a forest. Shear and buoyant production of TKE computed from the simulated resolved scale flow fields were principal sources in the upper canopy; the destruction of TKE due to canopy drag effects and the transfer to subgrid scales (dissipation) occurred primarily in the upper half of the forest where the foliage density was large; and turbulent transport showed a loss at the canopy top and a gain within the canopy. These general features have been found in various plant canopies in field experiments, higher-order closure models, and wind tunnel studies, but in all such studies, there is a lack of information concerning the pressure transport term.

Previous studies, both experimental and numerical, typically incorporated pressure effects into a residual term due to the difficulty in directly measuring turbulent pressure fluctuations and/or the lack of understanding on how to parameterize such terms. In the present LES study, the pressure was calculated directly; thus, the pressure transport term could also be calculated. Above the canopy, pressure transport appeared to balance approximately one-third of the turbulent transport, while near the canopy top and below pressure transport was the same sign as turbulent transport showing a sink near the canopy top and a source below. The transport terms accounted for over half of the TKE sink at the canopy top, and in the lowest two-thirds of the canopy the transport terms

were the dominant source terms in the budget. Moreover, the pressure transport was the largest source of turbulent kinetic energy in the lowest levels of the canopy. These results indicate that pressure transport is important in the plant canopy turbulent kinetic energy budget, especially in the lowest portion of the stand.

TABLE OF CONTENTS

1. Introduction

Turbulent kinetic energy budgets are used to study the relative importance of different physical processes that govern turbulent motions. The presence of a plant canopy in a boundary layer provides unique challenges for measurements, modeling, and understanding of the physical processes. Most notably, the plant canopy imposes an aerodynamic drag on the flow and creates turbulent motions in the wakes of the plant elements. This latter process is an additional source of turbulent kinetic energy, called wake production (Wilson and Shaw, 1977; Raupach and Shaw, 1982; Raupach *et al.*, 1986), but consideration must be given to the scale of motion generated in such wakes. In addition, the canopy may act as a heat source or sink, or both depending on the temperature difference between the layers of the canopy and the surrounding air at each level.

Lesnik (1974) provides an early picture of the plant canopy turbulent kinetic energy budget. Data from a twenty year old pine forest were analyzed under different stability conditions. In all three stability cases presented, the shear production was a large source at the canopy top where the wind shear gradient was the largest; the dissipation was a large loss in the upper canopy, while the turbulent transport showed a significant loss at the top of the canopy and a gain within the canopy. The buoyancy was small in comparison with the other terms and was not shown. The unique feature of the budget presented by Lesnik was the role of the turbulent transport term, where the large gain in the lower canopy levels represents an import of turbulent energy from the primary production region in the upper canopy levels.

Analyses of recent field experiments (Shi *et al.*, 1987; Leclerc *et al.*, 1990; Meyers and Baldocchi, 1991) support these results. Meyers and Baldocchi (1991) presented TKE budgets for a deciduous forest under neutral stability conditions. In the TKE budget the measured profiles of shear production and turbulent transport, and the dissipation, found as a residual, were in qualitative agreement with Lesnik (1974). Meyers and Baldocchi (1991) found that wake production slightly exceeds shear production at all levels within the canopy except near the canopy top.

The effects of atmospheric stability on the TKE budget were investigated in Shi *et al.* (1987) and Leclerc *et al.* (1990) using data from a deciduous forest collected during the Camp Borden experiment (Shaw *et al.*, 1988). The most dramatic changes were observed for stable conditions ($h/L \geq 0.25$) which were not simulated in the present LES study. In general, their measurements showed that normalized shear production and dissipation, found as a residual, increase with the onset of stability, and that buoyancy was a gain under unstable stratification and a loss in stable conditions. However, their measurements showed relatively little variation in the budget terms over the range of stability represented in the present study.

Leclerc *et al.* (1990) also presented the TKE budget in an alternative manner where the turbulent kinetic energy was split into two different scales, turbulent shear kinetic energy (SKE) and turbulent wake kinetic energy (WKE), following Shaw and Seginer (1985). This mathematical split was based on the constraint that total TKE was conserved. In presenting the budgets in this manner, the canopy now acts as a loss of kinetic energy on the "large" shear producing scales, and a gain in the "small" wake scales. This process represents the action of the drag elements to suppress turbulent motions as

well as the mean flow and, at the same time, to create small scale motions in the wake of plant elements. Profiles showed that the canopy drag was the primary destruction term in the SKE budget while shear production was the primary source in the upper canopy. The turbulent transport was a loss near the canopy top and a gain within the canopy. Most importantly, the residual term represented viscous dissipation, pressure transport and accumulated errors. Under unstable conditions, the residual was a gain within the canopy and a loss at the canopy top and above. Thus, pressure transport may be a source of SKE in the canopy and a loss above.

These field experiments contribute to our understanding of turbulent flow within a canopy; however, the effects of turbulent pressure fluctuations are still largely uncertain. Zhuang and Amiro (1994) provided stronger evidence as to the roles of the pressure perturbations in plant canopy flow. They evaluated the TKE budget during coherent motions in a deciduous forest using data collected during the Camp Borden experiment. The pressure perturbations were not measured due to the inherent difficulty in measuring static pressure perturbations; rather, they were calculated by taking the divergence of the momentum equation to form a Poisson equation for the perturbation pressure. The pressure derived in this manner neglects the contributions from the lateral derivatives due to the lack of measurements. Zhuang and Amiro cite several studies that support the contention that for coherent motions lateral effects are small in comparison to motions in the $x-z$ plane, and that pressure perturbations derived from the two dimensional field should account for most of the pressure effects in the budgets. In addition, the TKE budget presented was for an ensemble average of two dimensional coherent structures, as

a result the budget contained both longitudinal and vertical pressure transport terms. Budget profiles showed that the vertical pressure transport was a loss at the canopy top and a gain within the canopy, and longitudinal pressure transport was always a loss. Although the pressure perturbations have been difficult to ascertain within a plant canopy, several studies have measured surface pressure fluctuations.

Maitani and Seo (1985) measured surface pressure fluctuations in a wheat canopy and vertical velocity fluctuations within and above the canopy. They assumed that the pressure fluctuations in the canopy could be approximated by the surface pressure. Vertical plots of the measured pressure-velocity covariance and an integration of the pressure-velocity cospectrum over the analyzed frequencies were, in general, negative indicating that the pressure driven flux of TKE was downward. Their measurements showed that the pressure transport term in the TKE budget was not negligibly small. Shaw *et al.* (1990) and Shaw and Zhang (1992) used measured surface pressure fluctuations and velocity fluctuations measured during coherent motions in a forest to determine the role of pressure fluctuations in canopy turbulence. Shaw *et al.* (1990) compared surface pressure measurements to pressure fluctuations calculated through a Poisson equation to demonstrate that pressure fluctuations at the surface were primarily created by velocity perturbations in the high shear region near the top of the forest. Shaw and Zhang (1992) found that longitudinal velocities measured in the trunk space are strongly correlated with surface pressure, and that peak correlations occurred with near-zero time lag. Shaw and Zhang stated that this was strong evidence, but not proof, that turbulence at low levels in the forest is driven by pressure fluctuations. Pressure induced

motions in the lower canopy would account for a significant pressure transport term in the TKE budget.

An alternative to field experiments has been the use of closure models to investigate canopy budgets (Wilson and Shaw, 1977; Meyers and Paw U, 1986; Meyers and Paw U, 1987; Meyers and Baldocchi, 1991). Although these models give qualitative agreement with the profiles of shear production, wake production, destruction effects, and turbulent transport, pressure effects were either assumed negligible or parameterized. As a result, no conclusions can be drawn regarding the role of pressure perturbations in the budgets.

Wilson (1988) presented a higher order closure model using a different formulation. The turbulent kinetic energy budget was split into two different wavebands in a manner that was similar to the discussion in Shaw and Seginer (1985). The computed profiles where in qualitative agreement with Shaw and Seginer. As with other studies, the pressure transport term was assumed negligible, and no conclusions were made on the role of pressure fluctuations in the SKE budget. Wilson did find that the calculated level of wake kinetic energy had no feedback on the levels of shear kinetic energy, mean velocity, or Reynolds stress; therefore, he proposed that it was not necessary to include wake kinetic energy in his closure model.

Others have turned to wind tunnel studies to investigate the airflow within and above a plant canopy. Most notable are the studies of Raupach *et al.* (1986) and Brunet *et al.* (1994) for airflow in an artificial wheat canopy. Budgets were presented that are in qualitative agreement with field experiments and mathematical models. Moreover, both studies offer insight to the possible role of the turbulent pressure perturbations within and above a plant canopy. In the TKE budget, Raupach *et al.* (1986) found significant

differences between two calculations of the dissipation. They suggested that the difference may be due to the vertical pressure transport indicating that pressure transport was a source above the canopy in approximate balance with turbulent transport, and that pressure and turbulent transport were both sources of TKE within the canopy. The study of Brunet *et al.* (1994) also suggested that pressure transport was a source above the canopy. However, their residual analysis indicated that pressure transport was a loss within the canopy which contradicts the earlier results of Raupach *et al.* (1986). Brunet *et al.* (1994) cautioned that their analysis cannot be taken as proof, and due to the contradictions with Raupach *et al.* (1986) stated that "there is clearly an urgent need for high-quality measurements of fluctuating pressure in the context of plant canopy flows."

LES may have a partial answer to this call for measurements. For example, Moeng (1984) suggested that large-eddy simulations (LES) may be a way of obtaining "data" to study and understand the physical processes within the turbulent planetary boundary layer. The LES described in Moeng (1984) and later modified in Moeng and Wyngaard (1988) has been used for several planetary boundary layer flows (Moeng and Sullivan, 1994). The model has been tested for consistency against three LES codes written for the convective atmospheric boundary layer (Nieuwstadt *et al.*, 1993), in which the models were run for the same case and compared favorably. However, in the TKE budget for the simulated case, the pressure transport term was small and the scatter between models prevented any firm conclusions, but it was noted that some of the scatter was probably caused by an insufficient averaging period. Favorable results were obtained in Moeng and Wyngaard (1989) where they compared their simulated TKE budget to budget terms from a tank experiment (Deardorff and Willis, 1985) and aircraft observations (Lenschow *et al.*,

1980). Thus, LES proves to be a valid technique to study turbulent flows within the atmospheric boundary layer, and it is possible that LES may be adapted to plant canopy airflows.

Shaw and Schumann (1992) were the first to employ the LES technique to the plant canopy environment. Simulated mean velocity profiles, vertical profiles of Reynolds stress, turbulent kinetic energy, and velocity skewness qualitatively matched observations. Recently, Kanda and Hino (1994) used LES to explore coherent motions within and above a plant canopy; however, the simulation was for the developing stage of turbulence and not fully developed turbulent flow.

In this present study, the LES of Moeng (1984) and Moeng and Wyngaard (1988), as modified by Patton *et al.* (1994) to include a plant canopy, was used to generate model data. The motivation was to use the three dimensional output of velocity, temperature, subgrid scale kinetic energy, and pressure calculated through a Poisson equation to calculate *all* terms in the resolved scale turbulent kinetic energy budget with particular emphasis on determining the role of the pressure perturbations in the budget. Several simulations were run with different canopy specifications. Comparisons were made between simulations and with field experiments, closure models, and wind tunnel results.

2. Methods

2.1 Equations

LES explicitly calculates the large, or resolved, scales of a turbulent flow while the small scales, the subgrid scales, are parameterized. The assumption is made that the resolved scales contain most of the energy and are fairly insensitive to the effects of the subgrid scale parameterizations. The resolved scale is mathematically defined by applying a grid volume average or filter process to the variables of the governing equations (Leonard, 1974). In the current model the resolved scale was defined using a wave-cut off filter in the horizontal and a grid volume average in the vertical (Moeng and Wyngaard, 1988). The derivation of the resolved scale equations was presented in Moeng (1984); however, some details will be presented here for completeness, and new terms will be introduced to represent the presence of the plant canopy. Specifically, a form drag term and a canopy heat source are added to the resolved scale momentum and energy equations, respectively. With the Boussinesq approximations, the resolved scale conservation equations of mass, momentum, and energy for plant canopy flow are

$$\frac{\partial \overline{u}_i}{\partial x_i} = 0 \tag{1}$$

$$\frac{\partial \overline{u}_i}{\partial t} = -\overline{u}_j\left(\frac{\partial \overline{u}_i}{\partial x_j} - \frac{\partial \overline{u}_j}{\partial x_i}\right) + \frac{g}{\theta_o}\overline{\theta}\delta_{i3} - \frac{\partial P^*}{\partial x_i} - \frac{1}{\rho}\frac{\partial \langle \overline{p} \rangle}{\partial x_i}\delta_{i1} - \frac{\partial \tau_{ij}}{\partial x_j} + F_i \tag{2}$$

$$\frac{\partial \overline{\theta}}{\partial t} = -\overline{u}_j\frac{\partial \overline{\theta}}{\partial x_j} - \frac{\partial \tau_{\theta j}}{\partial x_j} + S \tag{3}$$

where the overbar represents the filtering process. When filtering the advection terms, it is necessary to partition the flow variables into a resolved scale part and a subgrid scale part;

such as, $u_i = \overline{u}_i + u_i'$, and, as a result, additional terms arise in the resolved scale equations (Leonard, 1974; Moeng, 1984). This is similar to additional terms arising when forming the traditional Reynolds decomposition.

In the momentum equation the additional terms appear as the subgrid scale stress tensor that is written as

$$\tau_{ij} = R_{ij} - R_{kk}\,\delta_{ij}/3 \tag{4}$$

where

$$R_{ij} = \overline{u_i' u_j'} \tag{5}$$

In equation (4) the normal components have been subtracted from the stress tensor, and an equal and opposite term is added to the pressure term which has the form of

$$P^* = \frac{\overline{p}''}{\rho} + \frac{R_{kk}}{3} + \frac{\overline{u}_j \overline{u}_j}{2} \tag{6}$$

where $\overline{p}''$ is the pressure deviation from the horizontal mean (represented by the double prime) since the mean pressure field has been separated from the resolved scale pressure in equation (2). The third term on the right hand side of equation (6) is the kinetic energy component of the advection term. The substitution of (6) into the resolved scale momentum equation gives (see Appendix A for more details on the derivations)

$$\begin{aligned}\frac{\partial \overline{u}_i}{\partial t} = &-\overline{u}_j\left(\frac{\partial \overline{u}_i}{\partial x_j} - \frac{\partial \overline{u}_j}{\partial x_i}\right) - \frac{\partial}{\partial x_i}\left(\frac{\overline{u}_j \overline{u}_j}{2}\right) + \frac{g}{\theta_\circ}\overline{\theta}\delta_{i3} - \frac{2}{3}\frac{\partial \overline{e'}}{\partial x_i} \\ &- \frac{\partial}{\partial x_i}\left(\frac{\overline{p}''}{\rho}\right) - \frac{1}{\rho}\frac{\partial \langle \overline{p} \rangle}{\partial x_i}\delta_{i1} - \frac{\partial \tau_{ij}}{\partial x_j} + F_i\end{aligned} \tag{7}$$

where $\overline{e'} \equiv R_{kk}/2$ is the subgrid scale (SGS) kinetic energy, and the variables in the conservation equations have the following meaning: $\overline{u}_i$ is the velocity component in the x_i direction, $\overline{\theta}$ is the potential temperature, $1/\theta_o$ is the volumetric expansion coefficient, and g is the gravitational acceleration. The density is given as ρ, while $\langle \overline{p} \rangle$ is the horizontal mean pressure. τ_{ij} is the SGS shear stress, and $\tau_{\theta j}$ is the SGS heat flux. The canopy effects of form drag and heat source are represented as F_i and S, respectively. The resolved scale conservation equations can be solved with a knowledge of the SGS kinetic energy, the SGS fluxes, and the canopy effects.

The subgrid scale kinetic energy was solved using a budget equation following the formulation in Deardorff (1980). The equation has the form

$$\frac{\partial \overline{e'}}{\partial t} = -\overline{u}_j \frac{\partial \overline{e'}}{\partial x_j} - \overline{u_i' u_j'} \frac{\partial \overline{u}_i}{\partial x_j} + \frac{g}{\theta_o} \overline{w'\theta'} - \frac{\partial \overline{u_i' \left(e' + p'/\rho_o \right)}}{\partial x_i} - \varepsilon - 2\frac{\overline{e'}}{\tau} \qquad (8)$$

where the terms on the right hand side represent: advection of SGS kinetic energy by the resolved scale velocity, shear production due to the action of SGS Reynolds stress on the resolved scale velocity gradient, SGS buoyancy production, SGS transport effects, and dissipation. Closure assumptions are necessary to solve equation (8). Specifically, downgradient diffusion was assumed for the SGS momentum $\left(R_{ij} = \overline{u_i' u_j'} \right)$ and heat $\left(\tau_{\theta j} = \overline{w'\theta'} \right)$ fluxes, and for the transport terms. Kolmogorov's hypothesis was used for the dissipation rate. It is believed that the resolved scale motions are insensitive to these parameterizations. The last term in (8) represents an enhanced dissipation rate due to the presence of the plant canopy modeled after Shaw and Schumann (1992). The term was

chosen to represent the removal of SGS kinetic energy by the action of canopy drag, and was based on the assumption that eddies created in the wakes of the plant elements are much smaller than the scale of the SGS eddies; therefore, the wake eddies dissipate rapidly making no contribution to turbulent kinetic energy.

Next, the SGS fluxes in the resolved scale equations were parameterized assuming that the fluxes can be represented by the resolved scale strain rates in the following manner

$$\tau_{ij} = -K_M\left(\frac{\partial \overline{u}_i}{\partial x_j} + \frac{\partial \overline{u}_j}{\partial x_i}\right) \tag{9}$$

$$\tau_{\theta j} = -K_H \frac{\partial \overline{\theta}}{\partial x_j} \tag{10}$$

where the SGS eddy diffusivities, K_M and K_H, were assumed functions of the subgrid scale kinetic energy and a dissipation length. Further details of the subgrid scale energy budget and the subgrid scale fluxes are found in Moeng (1984).

Finally, canopy effects, form drag and heating source, must be parameterized. The form drag of the momentum equation is not simply a body force that is added to the equation, rather the term represents the combination of viscous drag and a discontinuity in pressure across drag elements within the grid volume, and it is analogous to the form drag presented in Wilson and Shaw (1977) and Raupach and Shaw (1982). The form drag term was parameterized in a conventional manner as a product of a drag coefficient, cross-sectional body area, and the square of the time dependent velocity. The drag force in the x_i direction is

$$F_i = -C_d a(z) V \overline{u}_i \tag{11}$$

where V is the scalar wind speed; C_d is a drag coefficient assumed constant and equal to 0.15 according to measurements in a deciduous forest (Shaw *et al.*, 1988); and $a(z)$ represents the plant area density that varies in the vertical.

Since no attempt was made to simulate the thermal energy budget of the canopy, the canopy heat source term, represented by S, was constant in time and modeled after Shaw and Schumann (1992). The magnitude of the canopy heat source was fixed at the canopy top using a specified canopy top heat flux, and the source decays exponentially as a function of an extinction coefficient and the downward cumulative leaf area index. This describes the canopy as being the greatest source of heat in the upper levels where the solar radiation load is the greatest, and as a weaker source of heat in the lower canopy where solar radiation is attenuated.

2.2 Numerical model

The governing equations were integrated in time using the second-order Adams-Bashforth scheme with the horizontal derivatives evaluated using a pseudospectral method (Fox and Orszag, 1973), and the vertical derivatives evaluated using second-order centered finite differences. The boundary conditions for the conservation equations were periodic in the horizontal; the upper boundary was specified as a frictionless rigid lid with zero mass, momentum, heat, and SGS kinetic energy flux; and the bottom boundary employed the no-slip condition. The time step for the simulations was equal to 0.1 seconds and the grid spacing of 2 meters was equidistant in all directions. There were 96 x 96 horizontal grids and 31 vertical grids (representing a domain size of 192m x 192m x 60m) with the lowest one-third of the domain (10 grid points) occupied by a 20m tall

forest. The forest was defined as a vertical distribution of leaf area density. Figure 1 gives the two profiles used in this study. The profiles are defined as a sparse canopy, leaf area index (LAI) equal to 2, and a dense canopy with LAI = 5. The leaf area index is the vertical integration of the leaf area density from the surface to the canopy top.

The conservation equations were solved on a non-staggered horizontal grid and a staggered vertical grid. The vertical velocity, $\overline{w}$, the subgrid scale kinetic energy, $\overline{e'}$, and the leaf area density are defined at the surface and on equally spaced grids above ($\overline{w}$ level). The streamwise velocity, $\overline{u}$, the lateral velocity, $\overline{v}$, potential temperature, $\overline{\theta}$, and the dynamic pressure, P^*, are defined at a half grid point above the surface and the intermediate levels above ($\overline{u}$ level). The budget terms were calculated at the $\overline{u}$ level resulting in the budget terms being offset from the location of the leaf area density.

The LES was run for several different cases where the simulated flow was forced by treating the horizontal mean pressure gradient as an external forcing. The pressure gradient was adjusted at each time step to ensure a constant mass flux across the upwind $y-z$ plane where the mass flux was determined by defining a constant mean wind speed, U, at the upwind boundary. The mean wind speed was varied between simulations in order to study the environmental influences on the budget. The canopy density and the strength of the heat sources were also varied between simulations to determine canopy influences. As mentioned previously, two canopy densities were used in this study. In addition, the canopy heating source was represented as either a high sensible heat exchange or a low sensible heat exchange by specifying two different canopy top heat fluxes, $Q_* = 0.125$ and $0.005\ \ m\,K\,s^{-1}$. Table 1 summarizes environmental and canopy

forcing used in the simulations. The simulations are ordered in terms of a stability parameter h/L (Shaw *et al.*, 1988; Leclerc *et al.*, 1990) where h is the height of the canopy and L is the Monin-Obukov length evaluated at the canopy top.

After the flow reached equilibrium for a simulation, data sets were saved at a specified time interval (250s or 500s). A data set contains the three dimensional output of the resolved scale velocity ($\overline{u},\overline{v},\overline{w}$), the resolved scale potential temperature ($\overline{\theta}$), the SGS kinetic energy ($\overline{e'}$), and the dynamic pressure (P^*). However, to form the budgets it was convenient to recalculate the pressure perturbation field using a Poisson equation of the form

$$-\frac{\partial^2}{\partial x_i \partial x_i}\left(\frac{\overline{p}''}{\rho}\right) = \frac{\partial}{\partial x_i}\left\{-\overline{u}_j\left(\frac{\partial \overline{u}_i}{\partial x_j}-\frac{\partial \overline{u}_j}{\partial x_i}\right)-\frac{1}{2}\frac{\partial \overline{u}_j\overline{u}_j}{\partial x_i}-\frac{2}{3}\frac{\partial \overline{e'}}{\partial x_i}\right.$$
$$\left.-\frac{\partial\langle\overline{p}\rangle}{\partial x}\delta_{i1}+\frac{g\overline{\theta}}{\theta}\delta_{i3}-\frac{\partial \tau_{ij}}{\partial x_j}+F_i\right\} \qquad (12)$$

where the Poisson equation was obtained by taking the divergence of the resolved scale momentum equation. At this point *all* terms of the resolved scale TKE budget can be calculated.

2.3 The TKE budget equation

The derivation of the resolved scale TKE budget was similar to the traditional free atmosphere averaging procedures (Stull, 1988). Briefly, a horizontal mean momentum equation was derived by decomposing the flow variables in the resolved scale momentum equation (7) into a horizontal mean and a horizontal deviation. The horizontal mean momentum equation was obtained by taking the horizontal average of the decomposed

equation (see Appendix B). A horizontal perturbation momentum equation was then formed by subtracting the horizontal mean momentum equation from the resolved scale momentum equation (Appendix C). The canopy drag term was included in this analysis resulting in drag also reducing perturbation momentum. Thus, a TKE budget derived from the perturbation momentum equation also contains a term that acts to remove resolved scale TKE.

Wilson and Shaw (1977) specifically caution against such a formulation. They stated that adding a body force to represent canopy drag would satisfy the momentum equation, but such a term would not adequately describe other canopy effects (wake production) since drag would reduce turbulence as well as mean momentum from the flow. Instead, proper consideration of horizontal averaging and spatial differentiation could describe the canopy effects in the momentum equation and the TKE budget. The canopy effects would appear as a form drag term in the momentum equation, and the wake production process would naturally arise due to mathematical manipulation of the terms in the TKE budget (Wilson and Shaw, 1977; Raupach and Shaw, 1982; Raupach *et al.*, 1986).

In the present study, the above is not a concern since the numerical simulation specifically separates large and small-scale motions, and motions created in wakes behind canopy elements are assumed to reside in unresolved subgrid scales. Through the momentum equation, the canopy drag term acts to suppress resolved scale motions, and this influence is automatically carried through to resolved scale turbulent kinetic energy. The filter process defines the larger scales of the flow and sets a lower limit on the size of the resolvable eddies. Consequently, it was assumed that the wake production process

should occur on the subgrid scales, and a "wake destruction" process should occur on the resolved scales.

This assumption is similar to the ideas presented in Shaw and Seginer (1985). Shaw and Seginer stated that the total TKE could be viewed to consist of two components, the kinetic energy of the shear generated eddies and the kinetic energy of the eddies characteristic of the wakes of the canopy elements. This separation was based on the characteristic length scales of the eddies. The shear scale eddies had a length scale about one order of magnitude larger than the height above ground, and the wake eddies occurred on the scale of the plant elements. Shaw and Seginer state that there can be two orders of magnitude difference between the scales. This separation resulted in the canopy having opposing effects on the budgets, where the canopy acted as a sink for shear kinetic energy and a source for wake kinetic energy. In the present study, the resolved scales are analogous to the shear scale and the wake motions occur on the subgrid scales. However, as stated above, the assumption is made that wake production does not contribute significantly to the subgrid scales because wake scales are small and rapidly dissipate to heat.

The resolved scale TKE budget written in mixed notation for steady state, horizontally homogeneous conditions is

$$\frac{\partial\langle\overline{E}''\rangle}{\partial t} = 0 = \underbrace{-\langle\overline{u}''\,\overline{w}''\rangle\frac{\partial\langle\overline{u}\rangle}{\partial z}}_{P_s} + \underbrace{\frac{g}{\theta}\langle\overline{w}''\,\overline{\theta}''\rangle}_{P_b} - \underbrace{\left\langle\frac{\partial\overline{w}''\,\overline{E}''}{\partial z}\right\rangle}_{T_t} - \underbrace{\left\langle\frac{1}{\rho}\frac{\partial\overline{w}''\,\overline{p}''}{\partial z}\right\rangle}_{T_p} \tag{13}$$

$$+\underbrace{\langle\overline{u}_i''\,F_i''\rangle}_{D_{cd}} - \underbrace{\left\langle\frac{2}{3}\frac{\partial\overline{u}_i''\left(\overline{e'}\right)''}{\partial x_i} + \frac{\partial\,\overline{u}_i''\tau_{ij}''}{\partial x_j} - \tau_{ij}''\frac{\partial\,\overline{u}_i''}{\partial x_j}\right\rangle}_{D_{sgs}}$$

where $\langle\overline{E}''\rangle \equiv \langle\overline{u}_i''\overline{u}_i''/2\rangle$ is the horizontal averaged resolved scale turbulent kinetic energy (see Appendix D for more details on the derivation of the TKE budget). The angled brackets represent the horizontal average and the double prime represents the deviation therefrom. The perturbation momentum is defined as $\overline{u}_i'' = \overline{u}_i - \langle\overline{u}_i\rangle$. P_s is the mean shear production representing a conversion of mean flow kinetic energy to the resolved scale turbulent kinetic energy. This term is usually a source and is due to the interaction of the mean velocity gradients with the turbulent velocity field. P_b acts as either a buoyant production or destruction depending on the sign of the vertical heat flux. The heat flux is positive for unstable conditions representing a conversion of potential energy to TKE; and is a sink for TKE under stable conditions. T_t is the resolved scale turbulent transport, and T_p represents the vertical transport of resolved scale kinetic energy by the pressure fluctuations. D_{cd} is the parameterized influence of canopy drag. This term represents the rate of work performed by the velocity perturbations against the drag forces, and is identical to the canopy drag term in Shaw and Seginer (1985). D_{sgs} represents the combined effects of subgrid scale diffusion of resolved scale TKE (first two terms) and the

transfer of resolved scale TKE to the subgrid scales (last term). The subgrid scale diffusion effects were separated from D_{sgs} and added to the resolved scale turbulent transport (T_t), but, in general, their contribution was small. To avoid confusion with the resolved scale turbulent transport (T_t), the sum of resolved scale turbulent transport and subgrid scale diffusion is referred to as turbulent transport (TT). The transfer of resolved scale TKE to the subgrid represents a conversion of energy to the dissipation scales (Moeng, 1984; Mason, 1994). In this study, this is referred to as subgrid scale dissipation.

The budgets presented here are different from typical budget equations for the canopy layer (Wilson and Shaw, 1977; Raupach and Shaw, 1982; Raupach *et al.*, 1986). First, as noted above, there is no wake production term based on the belief that this process cannot be resolved in the current LES. This assumption is based on the fact that the grid resolution is two meters in the horizontal and vertical; thus, only eddies of wavelength greater than four meters can be resolved. Eddies of this size are significantly larger than the size of the eddies expected of the wake production process that occur on the scales of the plant elements (1-50 cm). Secondly, there are no dispersive fluxes (Raupach and Shaw, 1982; Raupach *et al.*, 1986). The dispersive fluxes represent spatial correlations between time averaged quantities; for example, at the edge of a tree stand a consistent downdraft may occur on the time average. This downdraft may be correlated with turbulent motions upwind of the edge, and the net effect would be a significant dispersive flux in the TKE budget. Dispersive fluxes are absent from the equations because the budgets are for only a spatial average, as opposed to performing a spatial or volume average in conjunction with a time average; however, an ensemble average of each term

was formed by averaging the terms over the number of available data sets within each simulation.

3. Results and Discussion

3.1 TKE budget profile

The normalized budget for the near neutral simulation (S5) is given in Figure 2. The overall features of the budget are in agreement with previous studies. Above the canopy there is an approximate local balance between the shear production and the rate of transfer of energy to the subgrid scales (dissipation). However, at the top of the domain shear production approaches zero due to the specification of a rigid upper boundary with no fluxes across the boundary. The subgrid scale dissipation remains an expected loss throughout the domain resulting in a local imbalance between production and dissipation. The imbalance is compensated for by turbulent transport that is unable to export kinetic energy through the upper lid. In previous experimental studies, turbulent transport was a maximum loss at the canopy top and remained a loss above the canopy decreasing in magnitude away from the top of the canopy. The positive values of turbulent transport above the canopy in this case appear to be an artifact of the boundary conditions.

Above $z/h \approx 1.3$ the pressure transport is roughly opposite the turbulent transport, and, in regions where the terms are not negligibly small, the magnitude of pressure transport is approximately 30% of the turbulent transport. The relative percentage of pressure transport to turbulent transport varies somewhat between simulations. This feature cannot be considered conclusive proof that pressure transport opposes turbulent transport above the canopy because of the possible boundary influences; however, the equilibrium between production and dissipation with a balance between the transport terms was inferred in the canopy wind tunnel study of Raupach *et al.* (1986).

There is considerable evidence that this balance occurs within the unstable atmospheric surface layer; for example, McBean and Elliott (1975) measured turbulent velocity components, temperature, and pressure at one height in the surface layer. The vertical profiles of the TKE budget terms were then inferred from Monin-Obukhov similarity using the measured data. Their results showed that the pressure transport was approximately equal to and opposite the turbulent transport. Brost et al. (1982) summarized several studies of the surface layer and the convective boundary layer that showed the pressure transport opposing turbulent transport. In the reported studies, pressure transport was determined as a residual and the percentage of pressure to turbulent transport varied from 50% in Lenschow et al. (1980) to 100% in Wyngaard and Coté (1971), Rayment and Chaughey (1977), and Chaughey and Wyngaard (1979).

McBean and Elliott (1975) proposed a simple model for the observed pressure transport profile based on measurements that showed the covariance $\langle \overline{w}'' \overline{p}'' \rangle$, using the current notation, and its vertical divergence were negative. These results indicated that the pressure and vertical velocity perturbations were of opposite sign and that the pressure transport was a source of turbulent energy in the lower levels. McBean and Elliott postulated that a local increase in perturbation pressure occurred below the maximum downward motion for a downward moving eddy in contact with the boundary, and the reverse occurred for an upward moving eddy that was in contact with the boundary. Both motions result in a negative covariance, and in order to have a negative vertical divergence, the covariance must become increasingly negative with height. McBean and Elliott do not comment on why this should occur; however, Wilczak and Businger (1984)

found that $\langle \overline{w}'' \overline{p}'' \rangle$ was increasingly negative with height using tower measured data for a series of temperature ramp structures.

Wilczak and Businger (1984) hypothesized that the pressure field retrieved from the momentum equations during the ramp structures should account for the pressure covariance term in the turbulent kinetic energy budget, and that the covariance became more negative with height was due to observed phase differences between pressure and vertical velocity associated with the measured inclined ramp structures. As a result, budget equations showed that pressure transport was a source of turbulent kinetic energy in approximate balance with turbulent transport. At this point it cannot be stated that ramp structures are responsible for the observed pressure patterns in the studies other than Wilczak and Businger (1984). Nevertheless, pressure transport appears to balance a percentage of the turbulent transport in the atmospheric surface layer and in the wind tunnel study of Raupach et al. (1986). It also appears that such a feature may occur above the simulated canopy presented here.

This result has been found in several numerical studies of the atmospheric boundary layer (e.g. Deardorff, 1980; Mason, 1989; Moeng and Wyngaard, 1989). Deardorff (1980) simulated the stratus capped convective mixed layer and found that pressure transport offset one-third to one-half turbulent transport except near the cloud base where the two terms were both sources of turbulent kinetic energy. Similar profiles were found in the convective boundary layer simulations of Moeng and Wyngaard (1989) and Mason (1989) where pressure transport roughly opposed turbulent transport throughout the boundary layer except just below the inversion base.

The approximate local equilibrium observed above the canopy, does not exist near the canopy top and below. In the upper canopy levels, shear production is the dominant source of turbulent energy due to the simulated large mean wind gradients. At the canopy top shear production is balanced by the destruction effects (canopy drag effects and SGS dissipation) and the transport processes. In fact, just above the canopy ($z/h=1.05$) turbulent transport and pressure transport account for over 50% of the TKE loss. Table 2 gives a summary of the ratios between the transport terms at the top of the canopy to the combined peak production. In all simulations, the transport terms account for a significant portion of the TKE loss.

Balance within the canopy occurs primarily between the loss due to the canopy drag effects and the gain due to shear production, turbulent transport, and pressure transport. However, shear production decreases quite rapidly becoming negligible below $z/h=0.65$; thus, turbulent transport and pressure transport serve as the primary TKE sources in roughly the lowest two-thirds of the canopy. Moreover, pressure transport is the primary source below $z/h\approx 0.5$ accounting for over 70% of the TKE source in the lowest third of the canopy. The significance of this effect is difficult to visualize when the transport terms are plotted on the scale of the largest budget terms; therefore, in order to better discern the effects of the budget terms, the individual terms have been plotted separately in the following section.

3.2 TKE budget terms

Shear production is the primary TKE production process in all simulations. Figures 3a and 3b show normalized shear production profiles for the simulations with leaf area index

of 2 and 5, respectively. The plot labels in the lower left of each figure are ordered in terms of increasingly negative values of the stability parameter h/L; thus, in Figure 3a case S1 is the least unstable, while case S4 is for the most unstable simulation. For ease of comparison the simulations with $h/L \geq -0.2$ will be referred to as the near neutral simulations, and when $h/L < -0.2$ the simulations will be referred to as the unstable simulations.

The general features of the normalized shear production for the sparse canopy (LAI = 2) show a peak in production at $z/h = 0.95$ and a fairly rapid decrease in the canopy (Figure 3a). The near neutral cases show some, albeit small, scatter among the simulations, and below $z/h \approx 0.80$ the profiles collapse to a similar profile. Moreover, the profiles for simulations S1 and S3 are in very good agreement (approximately 5%) throughout the domain. These simulations were for the same low canopy top heat flux, and the mean wind speed was varied from $2\ m\,s^{-1}$ in S1 to $1\ m\,s^{-1}$ in S3. Clearly these two profiles scale well when normalized in the conventional manner by h/u_*^3. A slightly larger difference is noted when comparing simulations S1 and S3 with simulation S2 (approximately 15%). In the latter case, the canopy top heat flux was large and the mean wind speed was increased to $4\ m\,s^{-1}$. Although the simulated profiles are within 10% agreement, the profiles suggest that the peak production is smaller for the high wind speed case which is physically unrealistic. Dimensional plots (not shown) reveal the expected order where the shear production rate is largest for the high wind speed case and decreases as a function of decreasing mean wind speed. The difference here may be due to the number of data sets analyzed. Time series traces of the canopy top friction velocity

showed considerable variability (Patton, personal communication), and, as a result, the number of data sets may not be sufficient to account for these variations. Small changes in friction velocity will have significant effect on profiles since the friction velocity is cubed when normalizing.

The largest differences in normalized production are observed between the near neutral simulations and the unstable simulation (S4). The unstable case had a high canopy top heat flux with a specified low mean wind speed. Normalized shear production is reduced by approximately 40%. Leclerc *et al.* (1990) found similar results where normalized shear production increased with the onset of stability. Based on the these results, one may conclude that shear production is smaller for the unstable case; however, this may not be true for all physical situations. For example, consider simulations S3 and S4 where both simulations had a specified low mean wind speed ($1\ m\ s^{-1}$), and the only difference between simulations was the canopy top heating. In dimensional form (not shown) the shear production was larger for the unstable simulation (S4). This is a consequence of the enhanced vertical motions due to the larger canopy heating. Although, the enhanced vertical motions will reduce the mean wind gradient, the vertical motions will also increase the flux of momentum within the canopy layer, and it appears that this increase in momentum flux is responsible for the larger shear production (dimensional form) observed in the unstable simulation. Added proof that the momentum flux has increased is seen by comparing the canopy top friction velocities (Table 1) where the friction velocity for S4 is approximately 40% larger than simulation S3.

The nondimensional profiles reveal the relative importance of shear production for a given simulation, and the small scatter between near neutral simulations indicates that similar physical processes account for turbulent kinetic energy production. For example, a comparison of peak shear production (for both normalized and dimensional form) to total peak TKE production reveals that shear accounts for over 98% of the total TKE production in the near neutral simulations, while in the unstable case shear production only accounts for approximately 75% of the total peak production.

The normalized shear production profiles for the dense canopy (LAI = 5) cases show features similar to the sparse canopy. Normalized peak production occurs at $z/h = 0.95$ (Figure 3b), and the near neutral profiles show some scatter collapsing to a single profile near $z/h \approx 0.85$. In addition, the normalized peak production is reduced by approximately 30% for the unstable case, and, for both simulated canopies, the profiles are not ordered strictly by the stability parameter, h/L. Although the profiles for both leaf area densities are similar, there are several notable differences due to the change in canopy density.

Normalized shear production is larger for the dense canopy, and, due to the aforementioned variations in friction velocity, a comparison was made with dimensional plots (not shown). The dimensional plots showed that the shear production rate was larger when only considering a change in canopy density. For example, the peak dimensional production for simulation S7 (dense canopy) was approximately 50% larger than simulation S3 (sparse canopy), and both production rates (in dimensional form) were much smaller than the other cases because the canopy heating and the mean wind speed were small. Further effects on shear production due to the change in canopy density can

be seen when comparing the near neutral simulations, where the normalized peak production value for the sparse canopy is approximately 6.5 while in the dense canopy the peak is about 8.5 representing a 30% increase. A similar increase is noted for the unstable simulations. These results indicate that the mean wind gradient is larger for the dense canopy. This is expected since the dense canopy will extract more momentum due to a greater canopy drag resulting in a larger difference between the canopy top and free-stream wind speed; however, the changes here may be influenced by the specification of a constant mass flux across the upwind edge of the model domain. For a given mean wind speed, a constant mass flux across the domain requires a stronger flow above the dense canopy since the dense canopy will reduce the airflow within the canopy layer, and the result being a larger mean wind gradient.

The normalized shear production profile in the dense canopy also shows a much more rapid decrease within the canopy. The dense canopy shear production becomes negligible, less than 10% of the canopy top peak, at a slightly higher level ($z/h \approx 0.65$) than in the sparse canopy ($z/h \approx 0.55$). Meyers and Baldocchi (1991) also found that normalized shear production decreased rapidly inside a deciduous forest with a leaf area index of 5. Their measurements showed production to be negligible below $z/h \approx 0.75$. The difference is likely due to the canopy architecture because the foliage was concentrated more in the upper levels of the forest reported in Meyers and Baldocchi (1991).

Figure 4 presents the profiles for normalized buoyant production where the profiles are, as expected, ordered in terms of the stability parameter. In general buoyancy is a negligible source when compared to shear production except in the unstable simulations

S4 and S8. Specifically, in the simulated unstable cases the peak buoyant production accounts for approximately 25% of the total peak production, and less than 2% of the total peak production for the near neutral simulations. The budget profiles presented in Leclerc *et al.* (1990) showed similar results where the normalized buoyant production was significant in their unstable case, and normalized buoyant production was negligible for their neutral measurements. The common features for both simulated canopies show that buoyant production is a maximum at $z/h_c \approx 1.05$, and is a source at all levels except for cases S8, S6, and S2 where buoyancy is a sink below $z/h \approx 0.45$. In the latter two cases the magnitude of the normalized sink is on the order of 10^{-3}.

The maximum buoyant production just above the canopy indicates that the vertical heat flux was large and positive at this level. This result is a direct consequence of the specified canopy heating profile. In the simulations, the canopy heating was largest at the top of the canopy and the heating exponentially decayed with decreasing height. Physically this represents solar radiation heating the leaves in the upper canopy which in turn heats the surrounding air given that no transpiration occurs. The decay into the canopy represents the strong attenuation of solar radiation resulting in the canopy acting as a weaker heat source.

The reversal of buoyancy from a production process to a destruction process occurs in the simulations that have a specified high canopy heat source (except case S4), and is only significant in case S8. Buoyant destruction occurs under thermally stable conditions when the vertical heat flux becomes negative. A stable layer develops within the simulated forest due to the specification of an elevated heat source resulting in the air in the upper

canopy to be the warmest with cooler air temperature below. Such a stable layer has been found to be typical of the daytime temperature profile within a canopy (Kaimal and Finnigan, 1994); however, the observed canopy heat flux is generally positive representing a countergradient flux of heat. The simulated downward heat flux may be an inadvertent consequence of the boundary conditions. The surface temperature was specified using a similarity relationship and the temperature at the lowest $\overline{u}$ level (a half grid point from the surface), while the upper boundary did not allow a flux of heat across the boundary. As a result heat was continually added to the system and thermal equilibrium was never reached. The continual source of heat in the upper canopy could result in the simulated downward heat flux; however, the simulated profiles are not unrealistic since the simulations are on the order of 10's of minutes and thermal equilibrium may not be reached on this time scale for certain atmospheric conditions.

The effect of the mean wind shear on buoyant production is seen by comparing simulation S4 to simulation S2 in the sparse canopy and by comparing simulation S8 to simulation S6 for the dense canopy. In these simulations the canopy top heat flux was large ($0.125\ m\,K\,s^{-1}$), and the mean wind speed was equal to $1\ m\,s^{-1}$ in simulation S4 (S8) with the mean wind increased to $4\ m\,s^{-1}$ in simulation S2 (S6). The canopy heat source is large, yet for the high wind case normalized buoyant production is small. Conversely, buoyant production was large when the canopy heating was large and mean wind small. These results may seem contradictory because for a given leaf area index and canopy heating rate one would expect that the rate of buoyant production in simulation S4 (S8) to equal buoyant production for simulation S2 (S6). In dimensional form (not

shown) the production rates are approximately equal, and, as with normalized shear production, the profiles in Figure 4 show the relative importance of normalized buoyant production to total production within each simulation.

The production processes are normally balanced by the destruction effects in the TKE budget. In the resolved scale TKE budget there are two destruction mechanisms, the SGS dissipation and plant canopy drag effects. The SGS dissipation represents the normal inertial cascade whereby large eddies are broken down into successively smaller eddies that are ultimately acted upon by viscosity. On the other hand, the canopy drag effects represent the direct removal of turbulent energy due to the interaction of resolved scale turbulence with the plant canopy. This process results in a short circuit of the normal eddy cascade (Shaw and Seginer, 1985).

Figure 5a presents the normalized SGS dissipation for the sparse canopy simulations. The dissipation is large at the canopy top and decreases within the canopy. As with shear production, the dissipation is not strictly ordered by the stability parameter. The near neutral simulations show little scatter between profiles, and normalized dissipation is approximately 50% larger than for the unstable case at the canopy top. In all cases the SGS dissipation is negligible (less than 10% of canopy top value) below $z/h \approx 0.60$.

The results for the dense canopy simulations are given in Figure 5b. The profiles are similar to the sparse canopy with the dissipation in the near neutral simulations approximately 50% larger than the dissipation in the unstable simulation at $z=h$. One notable difference is that there is less consistency between the near neutral simulations where SGS dissipation is the largest for the high wind speed simulation (S6). In addition,

the dissipation attenuates more rapidly in the dense canopy, and is essentially zero below $z/h \approx 0.55$. This is consistent with Shaw and Seginer (1985) who found the dissipation to be negligible within a dense corn canopy ($\mathrm{LAI} \approx 4.0$), while dissipation accounted for one-third of the loss in a sparse artificial wind tunnel canopy ($\mathrm{LAI} \approx 0.5$).

Shaw and Seginer (1985) also found that the action of plant canopy drag was the primary destruction process within their dense canopy. Similar results are found here (Figure 6). The general features show that the peak destruction occurs at $z/h \approx 0.85$ for all simulations, and destruction occurs primarily in the upper half of the canopy. Noted differences due to the canopy densities are larger peak destruction in the dense canopy simulations (Figure 6b), and the magnitude decreasing slightly more rapidly within the forest.

The primary differences occur between the near neutral simulations and the unstable simulations. The near neutral simulations show remarkable agreement throughout the canopy with a difference between profiles of less than 5%. The unstable simulations show greater destruction throughout most of the canopy. Leclerc *et al.* (1990) found that canopy drag was small in the lower portion of the forest, and approached zero with increasing stability in the lower half of the forest.

The transport terms of the resolved scale TKE budget can neither create nor destroy energy; rather, the transport mechanisms simply redistribute energy from one region to another. The general features of turbulent and pressure transport have already been presented in Figure 2. Here the details between simulations are presented, and the focus will be on the physical implications of the profiles near the canopy top and below.

The simulated turbulent transport profiles (Figure 7) show a loss at the canopy top and a gain within the canopy. The peak loss for all simulations occurs at $z/h=1.05$, and the average loss is roughly 35% of the combined peak production at $z/h=0.95$. Raupach *et al.* (1986) found that turbulent transport loss was approximately one-third of the combined production for the same level, $z \approx h$. The difference here is that the simulated turbulent transport profiles show a larger gradient in the upper canopy than the wind tunnel plots. This is probably due to the difference in canopy structure, where in the wind tunnel the leaf area density was constant with height in contrast to the structure in this study. The magnitude of the peak loss is very similar for both simulated canopies showing an average loss of -2.5 for the sparse canopy and -3.0 for the dense canopy; however, there appears to be no consistent ordering of the transport terms by the stability parameter.

In the canopy layer the profiles are roughly ordered in terms of the stability parameter. The sparse canopy simulations (Figure 7a) show little variability between profiles for the least unstable simulations (S1 and S2), and the normalized peak input of energy is largest for these simulations. Furthermore, the peak normalized turbulent transport source decreases for increasing instability. Clearly the peak source is ordered by h/L. In the lower half of the canopy, the near neutral simulations approach a similar value while turbulent transport is larger for the unstable simulation. The larger source corresponds to a larger gradient of the TKE flux. Leclerc *et al.* (1990) found that the flux of TKE increased for thermally unstable conditions, and normalized budget profiles showed a

larger turbulent transport source at the lowest measurement level in the forest for unstable conditions.

The dense canopy simulations (Figure 7b) show similar features. The peak source is ordered by the stability parameter. The near neutral simulations collapse to a single profile, and turbulent transport is slightly enhanced in the lower canopy for the unstable simulation; however, there are several differences in the turbulent transport profiles due to the change in canopy density. The turbulent transport peak is, on average, larger and occurs at a higher level in the dense canopy. The dense canopy profiles attenuate more rapidly with decreasing height, becoming negligible in the lowest one-third of the canopy. These features are consistent with increased normalized shear production for these simulations resulting in greater transport in the upper canopy, and the inability of vertical motions to penetrate into the dense canopy.

The turbulent transport terms plotted in Figures 7a and 7b contain two components. The first component is the resolved scale turbulent transport (T_t), and the second is the subgrid scale diffusion of resolved scale TKE. Figure 8 gives the components of the turbulent transport for simulation S4, where *TT* represents the sum of resolved scale turbulent transport and subgrid scale diffusion. In addition, the subgrid scale diffusion is spilt between normal and shear components represented as $S_n \left(= -\frac{2}{3}\partial \overline{u}_i''(\overline{e'})''/\partial x_i\right)$ and S_s $\left(= -\partial\ \overline{u}_i''\tau_{ij}''/\partial x_j\right)$, respectively. The resolved scale turbulent transport, T_t, is the largest component with subgrid scale diffusion generally less than 15% of the total (*TT*). Near the surface the normal component of subgrid scale diffusion is essentially zero, the shear component becomes negative, while the resolved scale turbulent transport is small and

positive. All simulations show these features where the negative values of turbulent transport are solely due to the shear components of subgrid scale diffusion, and the negative values are probably due to the subgrid scale parameterizations; however, further investigation is needed.

An encouraging aspect of the turbulent transport profiles simulated here is that the results are well supported by other studies. Field experiments for a pine forest (Lesnik, 1974) and from deciduous forests (Shi *et al.*, 1987; Leclerc *et al.*, 1990; Meyers and Baldocchi, 1991) all show this feature. This general profile has also been found in wind tunnel studies (Raupach *et al.*, 1986; Brunet *et al.*, 1994) and in higher order closure models (Wilson and Shaw, 1977; Meyers and Paw U, 1986, 1987; Meyers and Baldocchi, 1991). On the other hand, the second transport mechanism, pressure transport, is not as strongly supported in the literature.

The simulated effects of pressure transport (Figure 9) exhibit similar features as turbulent transport. Pressure transport is a loss between $0.8 \leq z/h \leq 1.3$ and a gain below $z/h \approx 0.8$; thus, for plant canopy turbulence, pressure transport also serves to transfer energy away from the primary production region, the upper canopy. Another similarity between transport profiles is that the peak loss at the canopy top and peak gain in the canopy are larger and occur at a higher level for the dense canopy simulations. The pressure transport profiles are not ordered by h/L in the upper canopy, but, below $z/h \approx 0.6$ (sparse canopy) or $z/h \approx 0.8$ (dense canopy), the most unstable cases show substantially greater values of pressure transport.

A significant difference between transport turbulent and pressure transport is that pressure transport does not attenuate as rapidly with decreasing depth into the canopy. In addition, pressure transports for the near neutral simulations in both canopies collapse to a similar profile below $z/h \approx 0.6$. In the lower canopy the primary balance of the resolved scale TKE budget is between the loss due to canopy drag effects and the gain due to turbulent and pressure transport with pressure transport accounting for most of the kinetic energy gain. Table 3 lists the average ratio of resolved scale turbulent transport to pressure transport from the level where pressure transport first exceeds turbulent transport. Pressure transport accounts for approximately 60% of the transport in the lowest third of the sparse canopy, and for approximately 70% of the transport in the lower half of the dense canopy. This result supports the belief that pressure transport is not negligible in the TKE budget and that pressure transport is a source of TKE in the canopy (e. g. Maitani and Seo, 1985; Shaw and Zhang, 1992; Raupach *et al.*, 1986; Leclerc *et al.*, 1990); however, this result contradicts the results of Brunet *et al.* (1994) where pressure transport was estimated to be a loss within the canopy.

Brunet *et al.* (1994) calculated the profiles of shear production and turbulent transport from measured wind tunnel data for an artificial wheat canopy. The dissipation was found using the measured u spectra, and a wake production term was calculated using the formulation presented in Raupach *et al.* (1986). Pressure transport was believed to be the dominant term in the residual. The residual showed a gain just above the canopy and a significant loss within the canopy indicating a severely unbalanced budget. Brunet *et al.* proposed that a "wake dissipation" term should be included in their original budget based

on the assumption that their measurements could not resolve the wake production process. The wake dissipation term was equal and opposite to the wake production and it was added to the viscous dissipation, but their wake dissipation term only accounted for the dissipation of "wake turbulence" by the mean wind and not for the turbulent energy destroyed by canopy drag. The new dissipation rate (*dissipation = viscous + wake dissipation*) gave results very similar to Raupach *et al.* (1986). However, the new residual still showed pressure transport as a TKE sink within the canopy, and this new residual was almost identical to the semi-empirical relationships of Zeman and Lumley (1976) and Deardorff (1973). Brunet *et al.* (1994) noted that this consistency cannot be taken as proof "since the closure assumptions are mostly empirical"; however, no explanation was given as to the observed agreement.

The agreement between the surface layer pressure transport parameterization and the new residual may not be valid for the plant canopy because the semi-empirical relationships were derived for a smooth, constant flux boundary layer. Both conditions are violated in the plant canopy; however, a possible test of the of the semi-empirical relationships would be to calculate the Deardorff (1973) parameterization with the LES data.

Finally, the residual term (Figure 10) in the resolved scale TKE budget represents any numerical errors, or an insufficient number of data sets used to form the ensemble average of the budget terms. The residual is largest at the canopy top where the other terms of the budget are large, but on average the maximum residual is less than 2% of the of the shear production for the corresponding level in the upper canopy. This small residual is

encouraging and indicates that numerical errors are negligible, and that the number of data sets averaged are sufficient to determine the terms of the resolved scale TKE budget. In addition, the assumptions of steady state and horizontal homogeneity have been satisfied, and it appears that not including a wake production term in the SGS kinetic energy equation has had little effect on the resolved scales. A possible reason for this is that eddies produced due to the wake production process dissipate rapidly (Raupach and Shaw, 1982; Wilson, 1988).

4. Summary and Conclusions

LES output has been used to calculate all terms of the resolved scale TKE budget for airflow within and above a forest canopy. The TKE budget contains the traditional terms that represent shear and buoyant production, turbulent transport, and pressure transport; however, differences arise because the budget is for the resolved scales of a LES. These scales are mathematically defined using a numerical filter process that separates the resolved scales of motions from the subgrid scale motions. A formulation in this manner sets a lower limit on the size of the resolvable eddies. As a consequence, the wake production term which is commonly found in a plant canopy budget does not appear in the resolved scale budget presented here; rather, the budget contains a term that represents a direct extraction of turbulent energy by the action of plant canopy drag. In addition, the traditional viscous dissipation effects are represented as a transfer of energy from the resolved scales to the subgrid scales by a parameterized shear stress term.

Several simulations were run using different environmental forcing and plant canopy specifications. The environmental forcing was specified through a mean pressure gradient that was adjusted during a simulation to ensure that a specified mass flux was maintained across the upwind boundary. The plant canopy was defined as either a sparse canopy (LAI = 2) or a dense canopy (LAI = 5), and the effects of canopy heating on the surrounding air were specified using a canopy top heat flux. A canopy heating rate profile was calculated from this heat flux to represent a high or a low solar radiation load on the forest. The thermal stability of a simulation was defined by a stability parameter of the

form h/L, where h is the canopy top and L is the Monin-Obukhov length; however, there was not always a clear order of the budget terms by the stability parameter.

The effect of canopy density changes were seen in all profiles. The simulated profiles showed that the normalized peak value of a budget term was larger in the dense canopy simulations. For example, normalized shear production for the dense canopy simulations were approximately 30% larger than the sparse canopy simulations. This feature was also observed in the normalized profiles of buoyant production, canopy drag effects, dissipation, and the transport terms. In addition, the dense canopy simulations showed that the magnitude of the budget terms attenuated much more rapidly within the canopy. This indicated that turbulent motions are suppressed in the lower portions of a dense forest when compared to a more open forest.

The most significant aspect of this study was that the three dimensional pressure perturbation field was numerically calculated; thus, allowing the calculation of the pressure transport term at all levels in the domain, and the effects of pressure transport could now be compared to the other budget terms for the first time. The general features of the budget showed, that above the canopy, there was an approximate balance between production and subgrid scale transfer (dissipation), and there were indications that turbulent and pressure transport roughly opposed each other with pressure transport balancing approximately 30% of turbulent transport; however, there was considerable variation between simulations. This approximate balance did not exist near the canopy top and below. At the canopy top, production was balanced by plant canopy drag effects, the energy transfer to the subgrid scales (dissipation), and by both transport mechanisms,

where turbulent and pressure transport counteracted over half of the production in the simulations. In the lowest two-thirds of the canopy, production and subgrid scale transfer became negligible, and the primary balance was between the loss due to canopy drag effects and the gain due to transport. Further, pressure transport was the dominant source in the lowest levels of the forest. In fact, pressure transport accounted for approximately 60% of the TKE source in the sparse canopy and roughly 70% of the source in the dense canopy.

TABLE 1. Plant canopy variables and forcing for simulations.

Simulation	LAI	Q* (ms^{-1} K)	U (ms^{-1})	h/L	u_* (ms^{-1})	Data Sets
S1	2.0	0.005	2.0	-0.024	0.388	15
S2	2.0	0.125	4.0	-0.074	0.767	13
S3	2.0	0.005	1.0	-0.185	0.196	15
S4	2.0	0.125	1.0	-1.398	0.281	12
S5	5.0	0.005	2.0	-0.017	0.424	12
S6	5.0	0.125	4.0	-0.064	0.801	12
S7	5.0	0.005	1.0	-0.153	0.209	06
S8	5.0	0.125	1.0	-1.252	0.302	08

Q* = canopy top heat flux; U = mean wind speed; h = canopy height;
L = canopy top Monin-Obukov length; u_* = canopy top horizontal mean friction velocity

TABLE 2. Ratio of turbulent transport ($TT_{\min}$) and pressure transport ($T_{p\min}$) peak loss at the canopy top to the combined shear and buoyant peak production ($P_s + P_b$).

Simulation	$TT_{\min}/(P_s + P_b)$	$T_{p\min}/(P_s + P_b)$
S1	0.39	0.13
S2	0.32	0.15
S3	0.43	0.11
S4	0.42	0.12
S5	0.38	0.13
S6	0.35	0.13
S7	0.37	0.14
S8	0.40	0.17

TABLE 3. Average ratio of resolved scale turbulent transport (T_t) to pressure transport (T_p). The average is calculated over the region from the surface to the level (z/h) where pressure transport first becomes larger than resolved scale turbulent transport.

Simulation	z/h	T_t/T_p
S1	0.35	0.42
S2	0.35	0.45
S3	0.35	0.29
S4	0.45	0.43
S5	0.55	0.27
S6	0.55	0.30
S7	0.65	0.30
S8	0.65	0.25

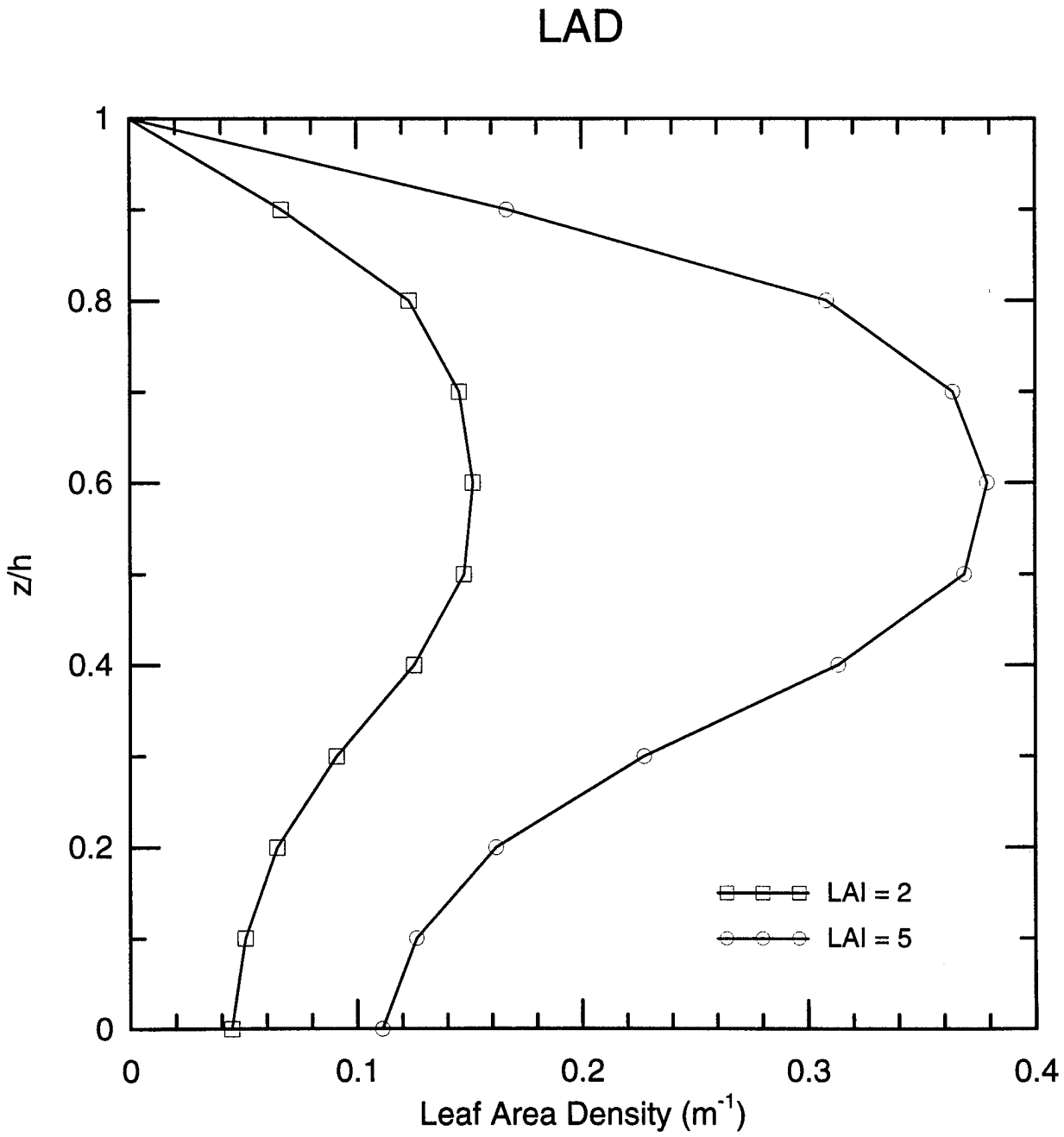

Figure 1. Vertical distribution of leaf area density (m^{-1}). Integration gives leaf area index (LAI) of 2 and 5.

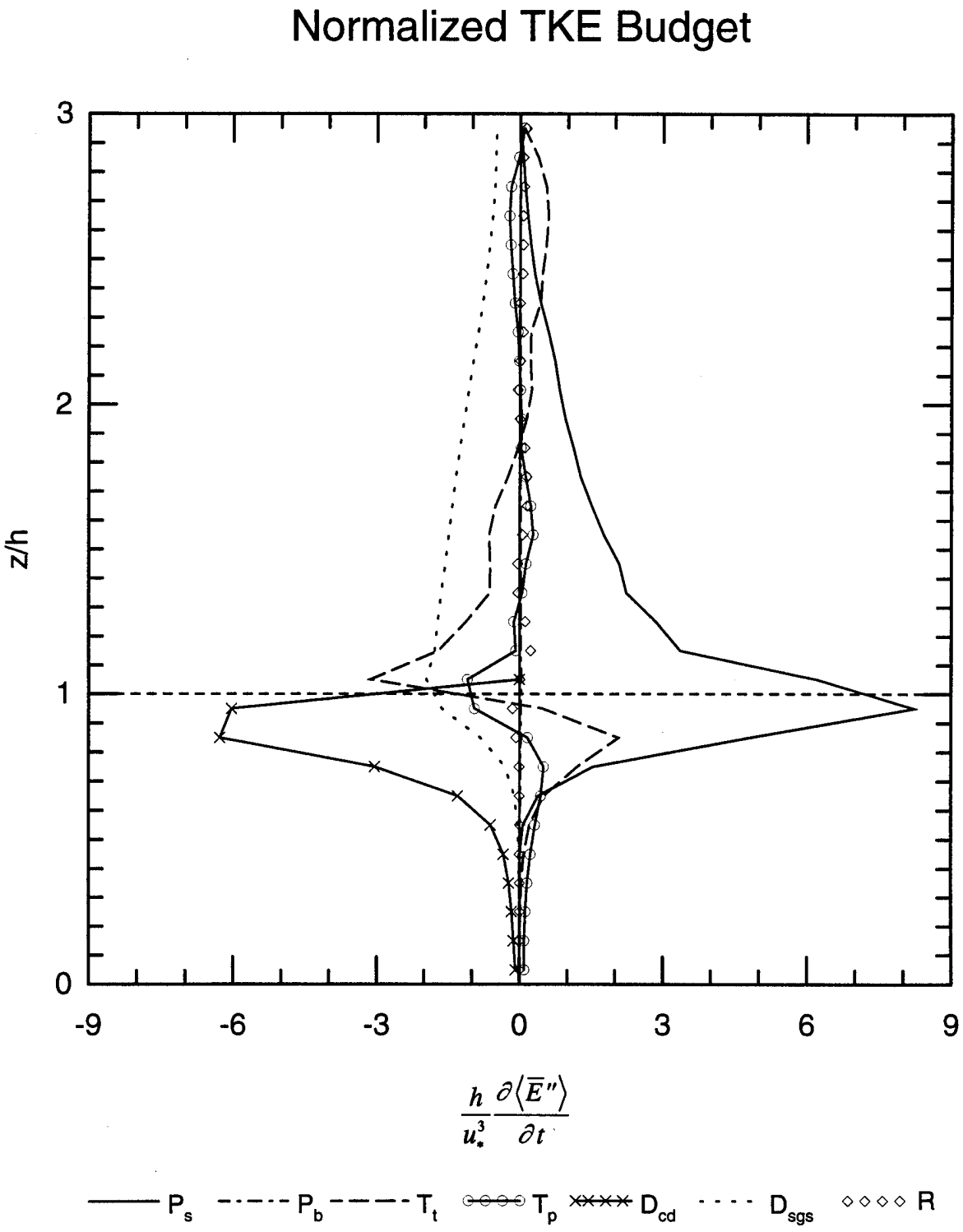

Figure 2. Normalized resolved scale TKE budget for simulation S5, $h/L=-0.017$. Plot labels refer to budget terms in equation (13), and R represents the residual.

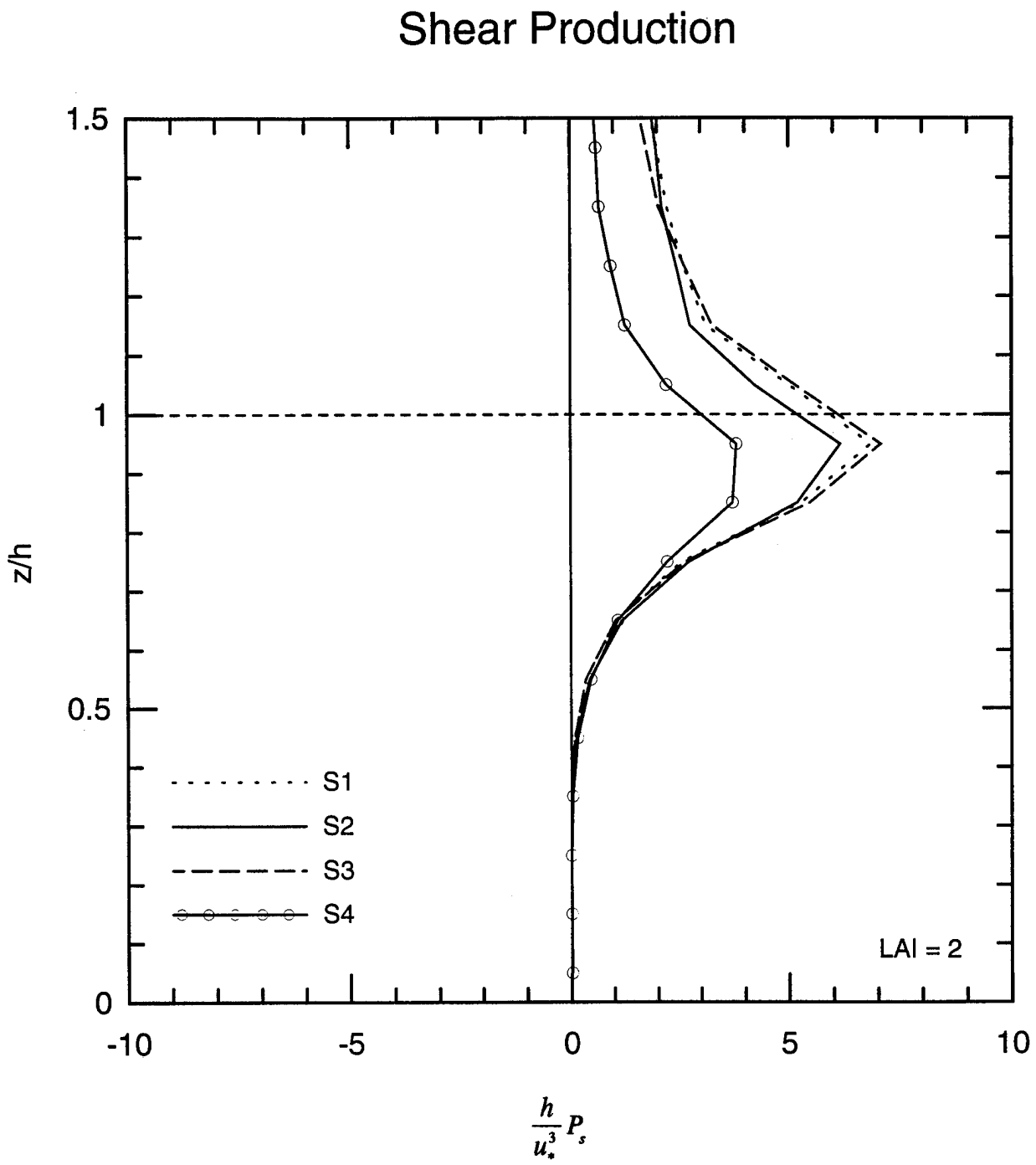

Figure 3a. Normalized shear production (P_s) for a sparse canopy LAI = 2. Plot labels are ordered in terms of increasingly negative h/L ; S1 ($h/L = -0.024$), S2 (-0.074), S3 (-0.185), S4 (-1.398).

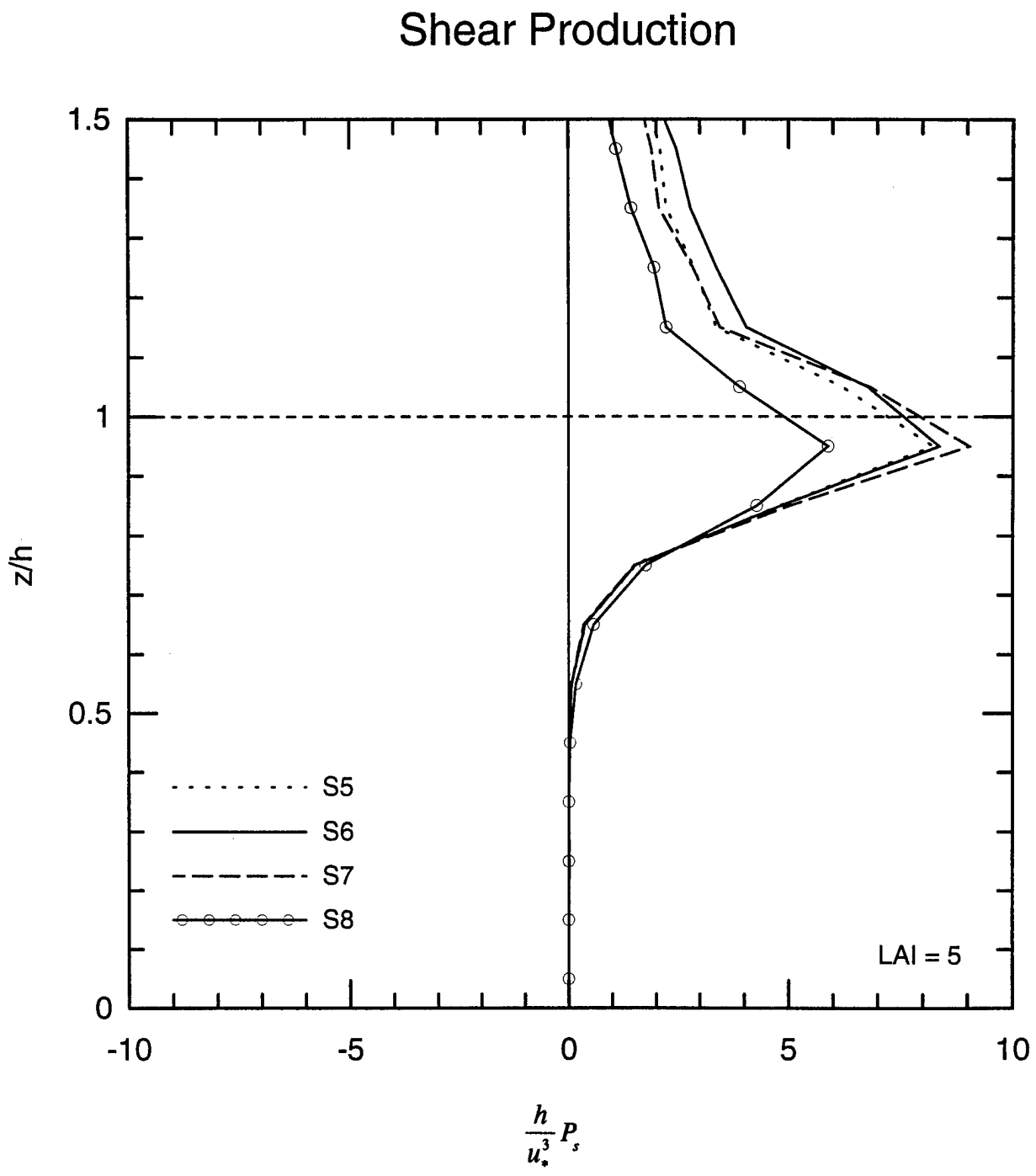

Figure 3b. Normalized shear production (P_S) for a dense canopy LAI = 5. Plot labels are ordered in terms of increasingly negative h/L ; S5($h/L = -0.017$), S6(-0.064), S7(-0.153), S8(-1.252).

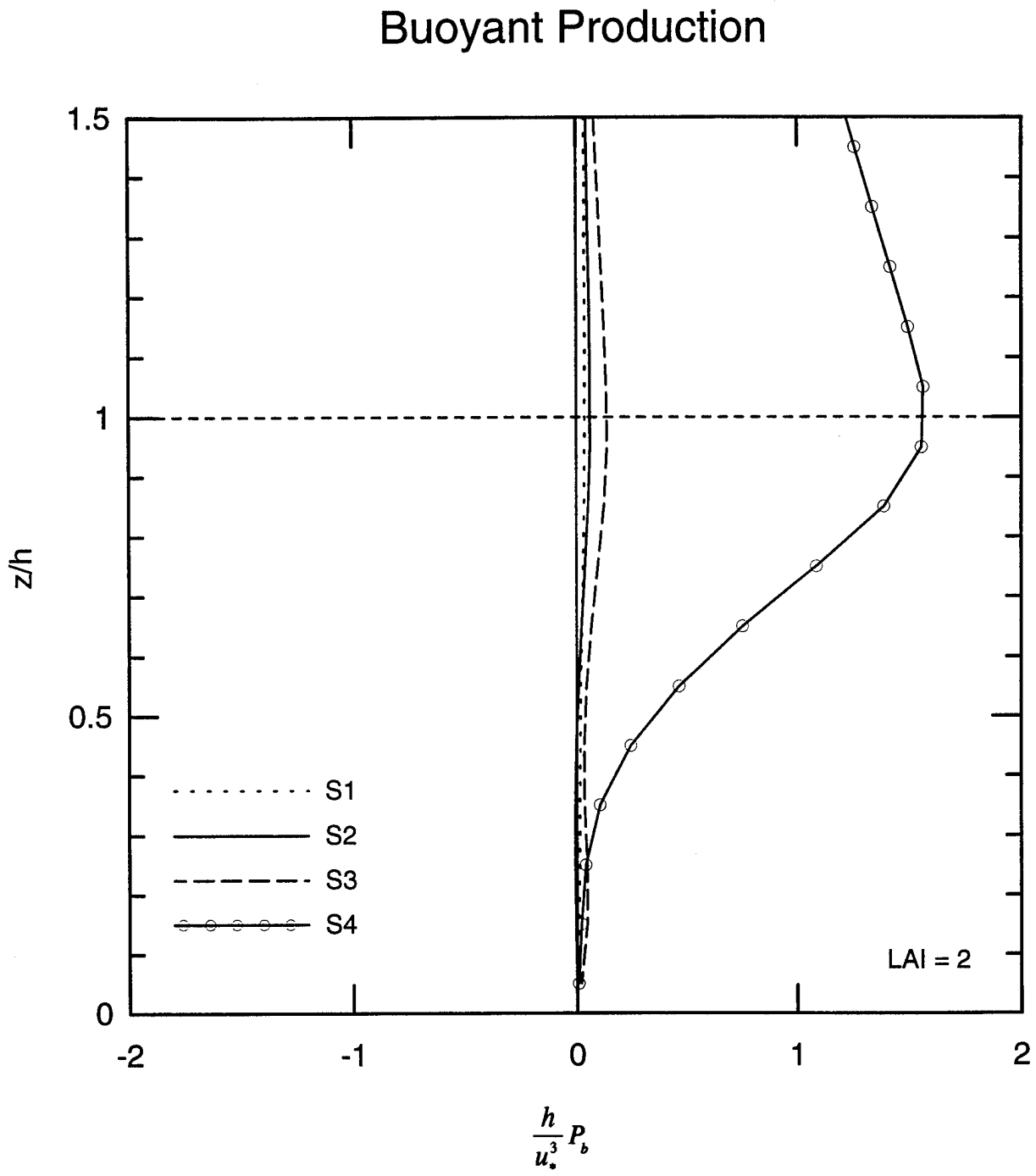

Figure 4a. Normalized buoyant production (P_b) for a sparse canopy LAI = 2. Plot labels are ordered in terms of increasingly negative h/L; S1 ($h/L = -0.024$), S2 (−0.074), S3 (−0.185), S4 (−1.398).

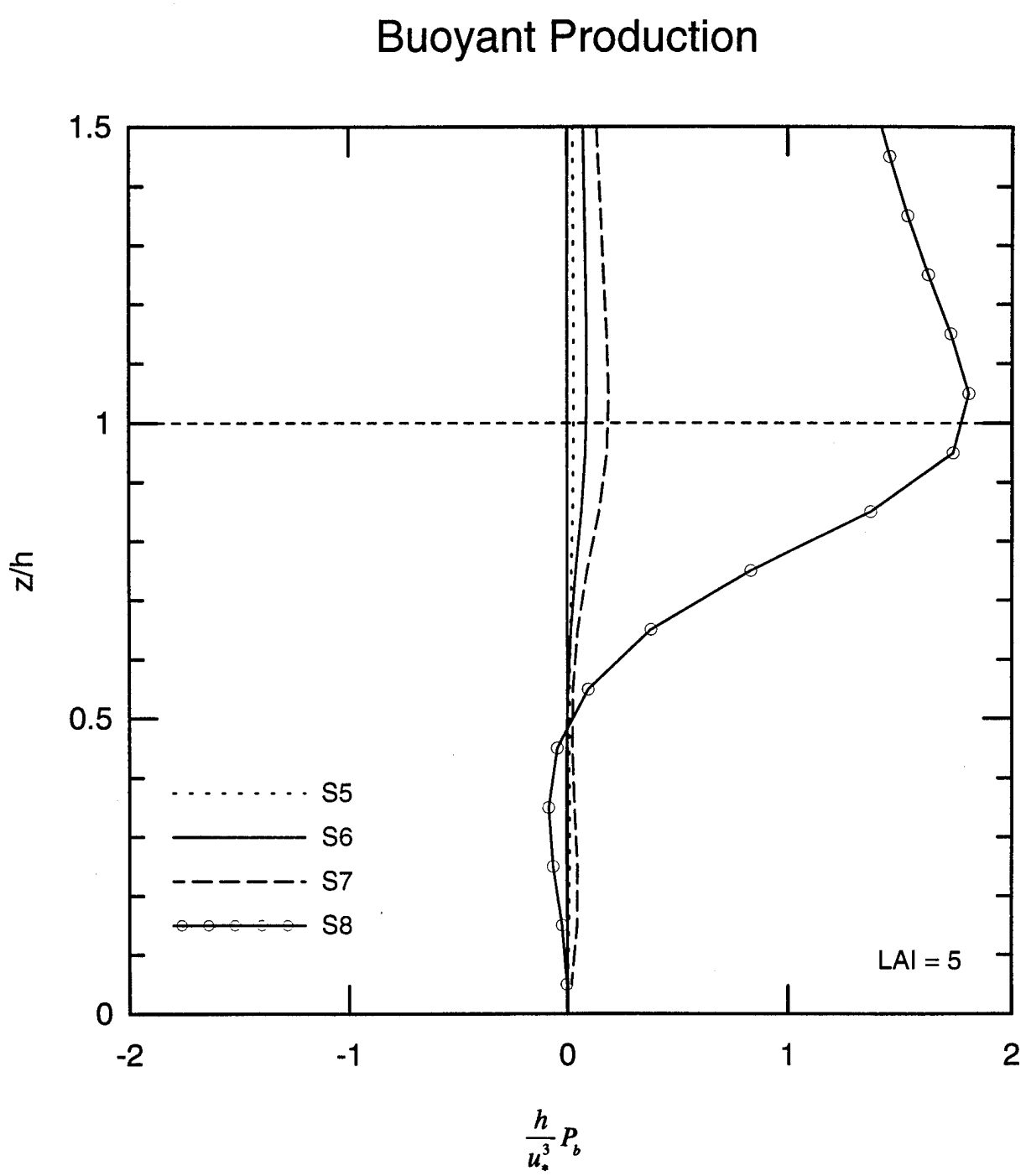

Figure 4b. Normalized buoyant production (P_b) for a dense canopy LAI = 5. Plot labels are ordered in terms of increasingly negative h/L ; S5($h/L = -0.017$), S6(-0.064), S7(-0.153), S8(-1.252).

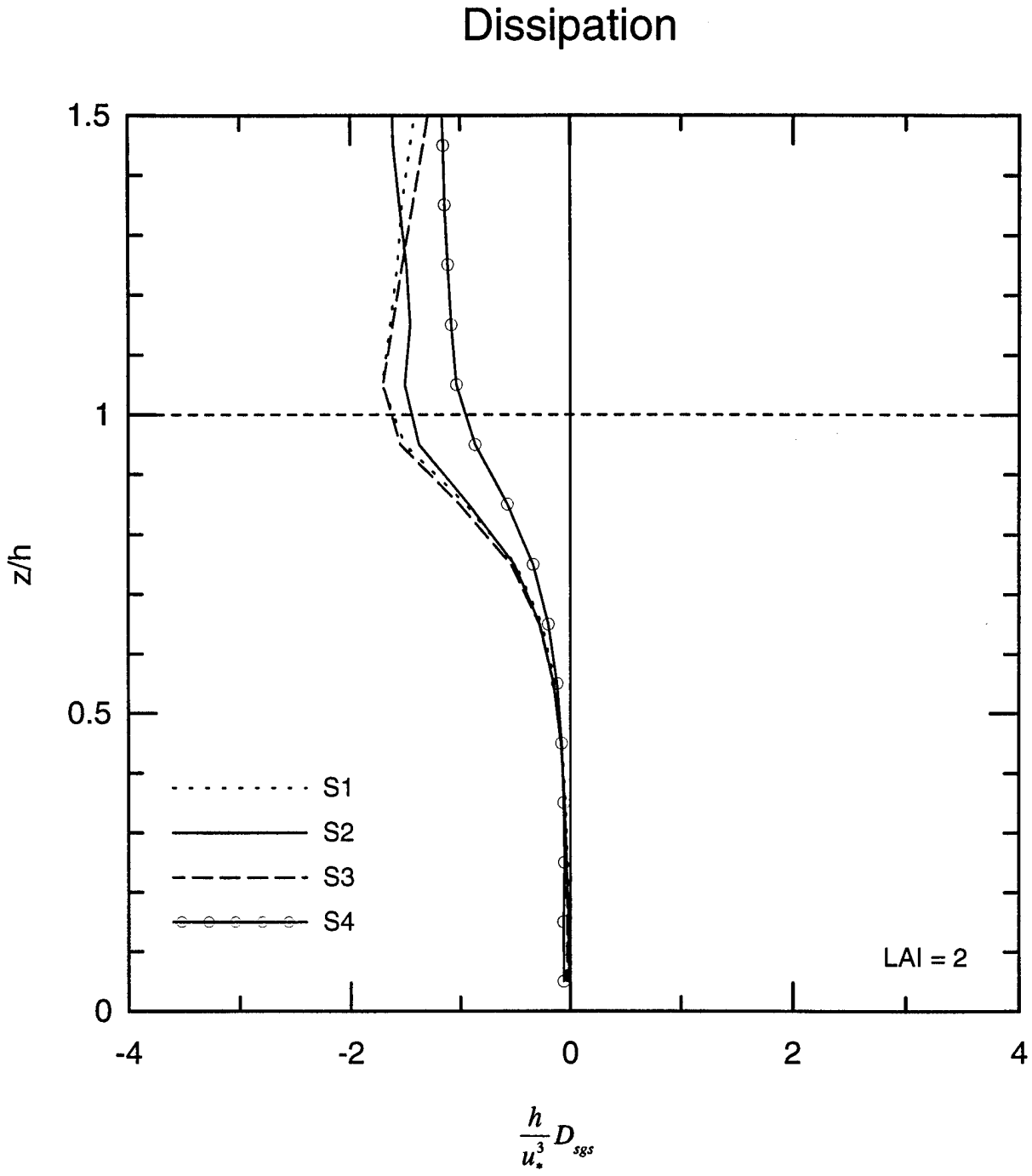

Figure 5a. Normalized SGS dissipation (D_{sgs}) for a sparse canopy LAI = 2. Plot labels are ordered in terms of increasingly negative h/L; S1 ($h/L = -0.024$), S2 (-0.074), S3 (-0.185), S4 (-1.398).

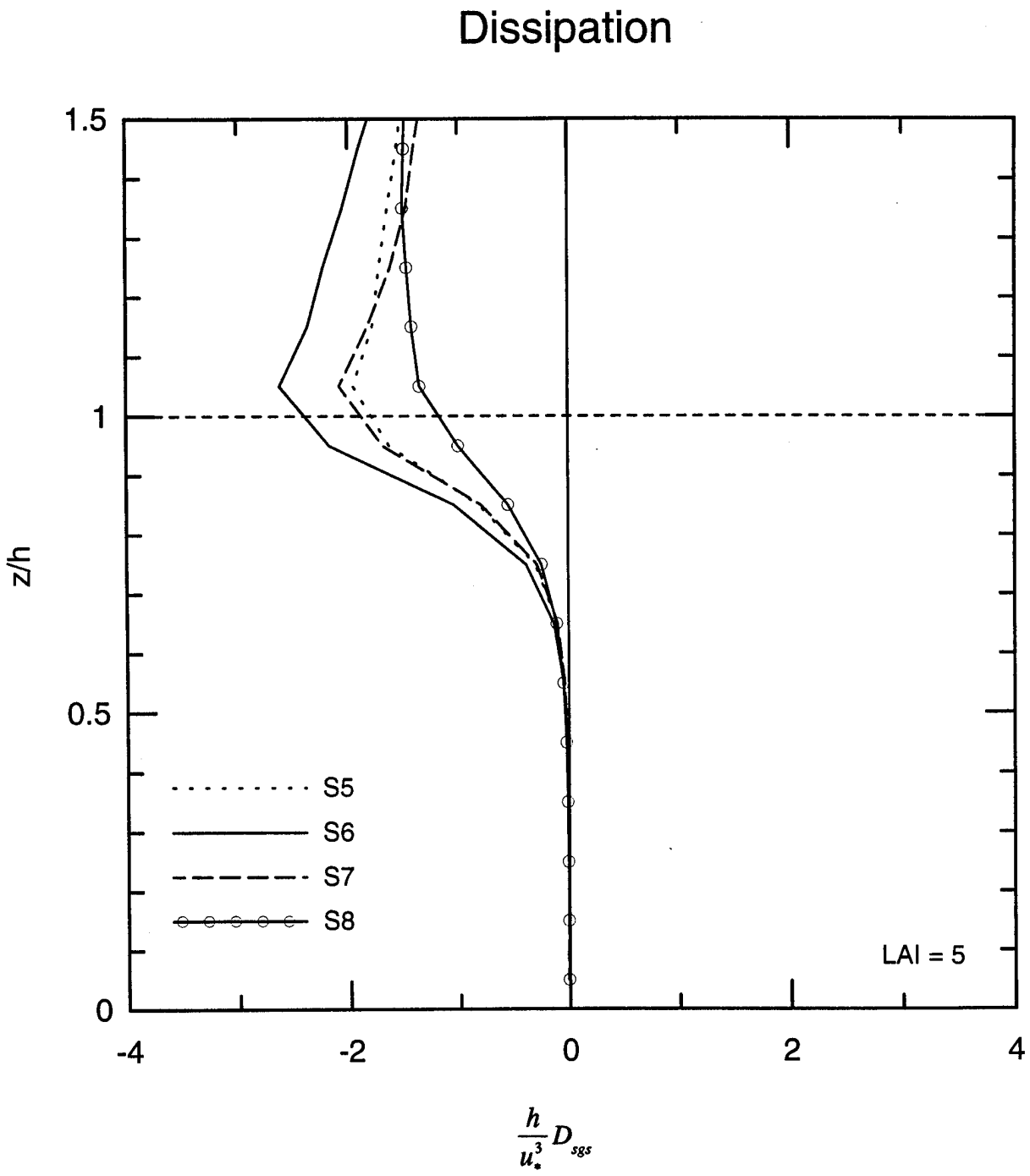

Figure 5b. Normalized SGS dissipation (D_{sgs}) for a dense canopy LAI = 5. Plot labels are ordered in terms of increasingly negative h/L; S5($h/L = -0.017$), S6(-0.064), S7(-0.153), S8(-1.252).

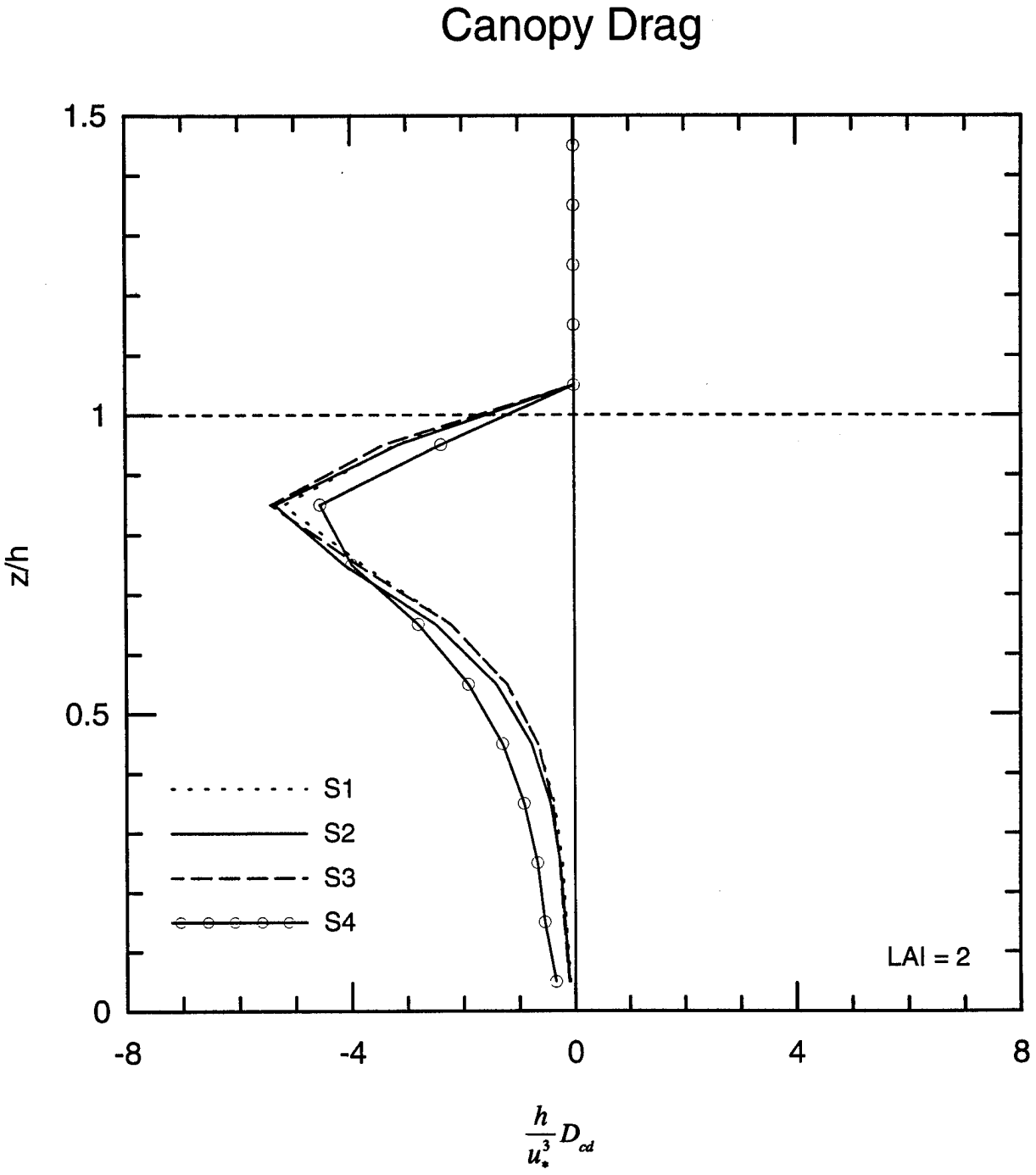

Figure 6a. Normalized canopy drag effects (D_{cd}) for a sparse canopy LAI = 2. Plot labels are ordered in terms of increasingly negative h/L ; S1 ($h/L = -0.024$), S2 (-0.074), S3 (-0.185), S4 (-1.398).

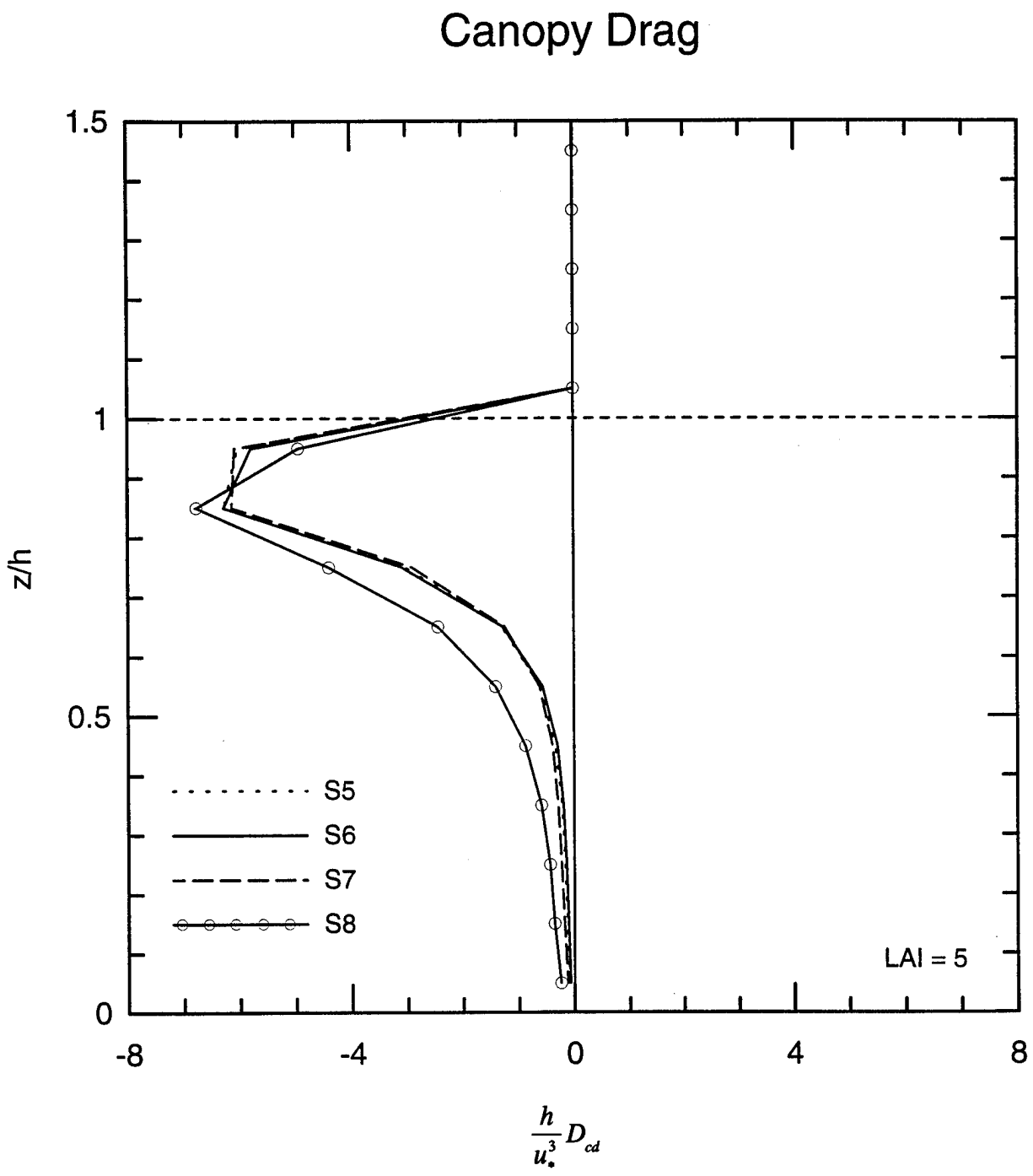

Figure 6b. Normalized canopy drag effects (D_{cd}) for a dense canopy LAI = 5. Plot labels are ordered in terms of increasingly negative h/L; S5($h/L = -0.017$), S6(-0.064), S7(-0.153), S8(-1.252).

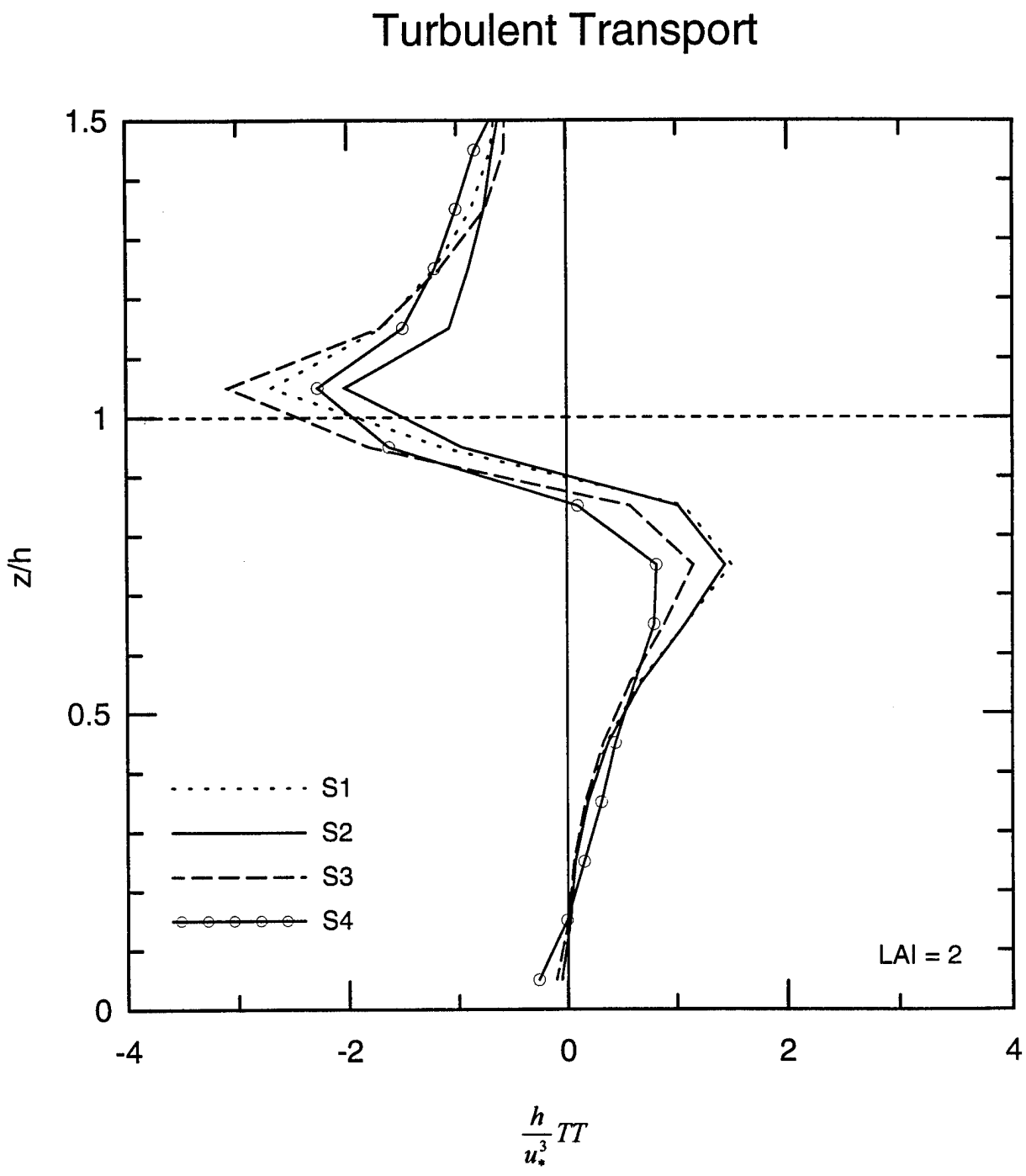

Figure 7a. Normalized turbulent transport (TT) for a sparse canopy LAI = 2. Plot labels are ordered in terms of increasingly negative h/L; S1 ($h/L = -0.024$), S2 (-0.074), S3 (-0.185), S4 (-1.398).

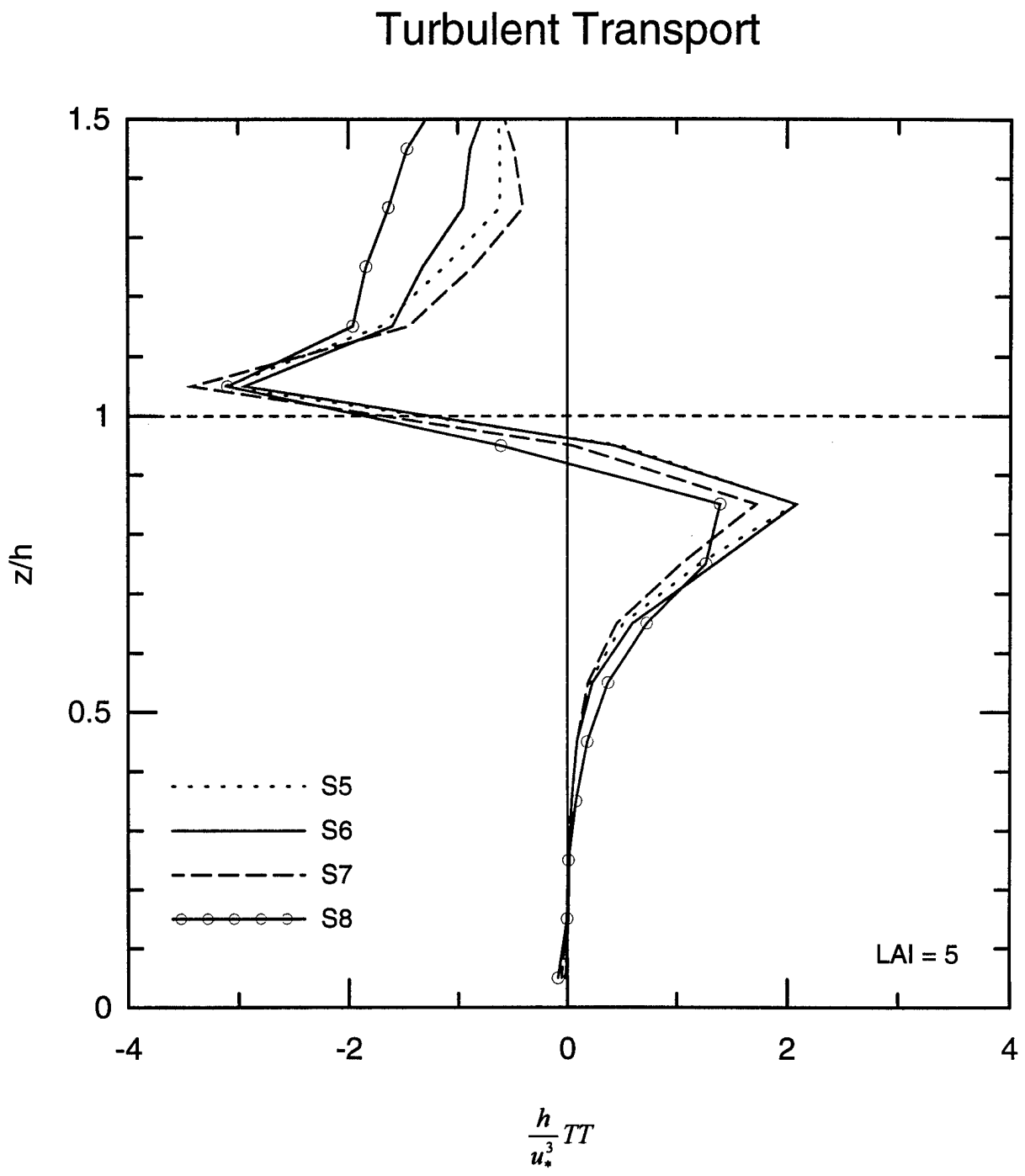

Figure 7b. Normalized turbulent transport (TT) for a dense canopy LAI = 5. Plot labels are ordered in terms of increasingly negative h/L; S5($h/L = -0.017$), S6(-0.064), S7(-0.153), S8(-1.252).

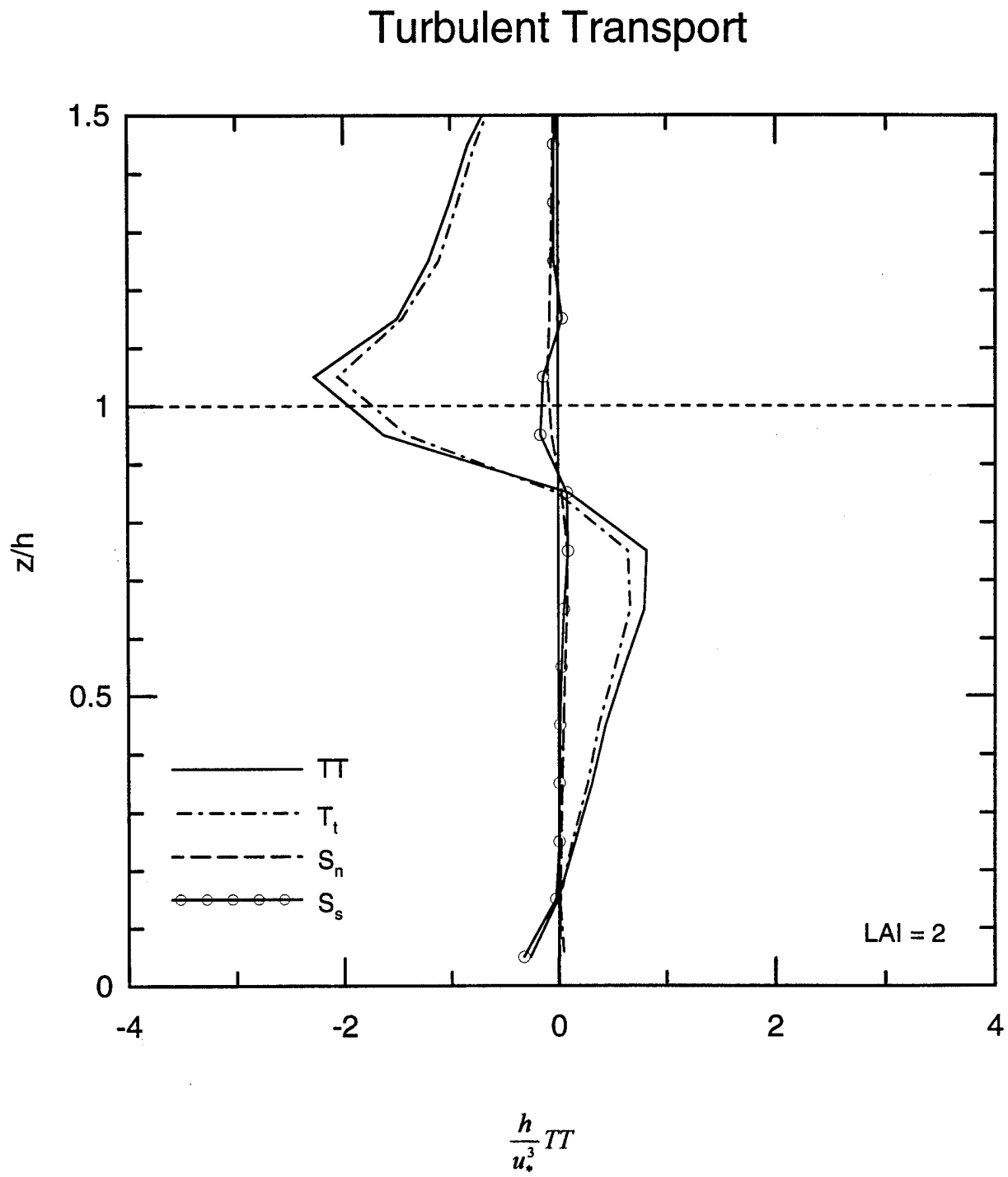

Figure 8. Normalized components of the turbulent transport term (TT) for simulation S4. T_t is the resolved scale component. S_n and S_s represent the normal and shear components of subgrid scale diffusion of resolved scale TKE, respectively.

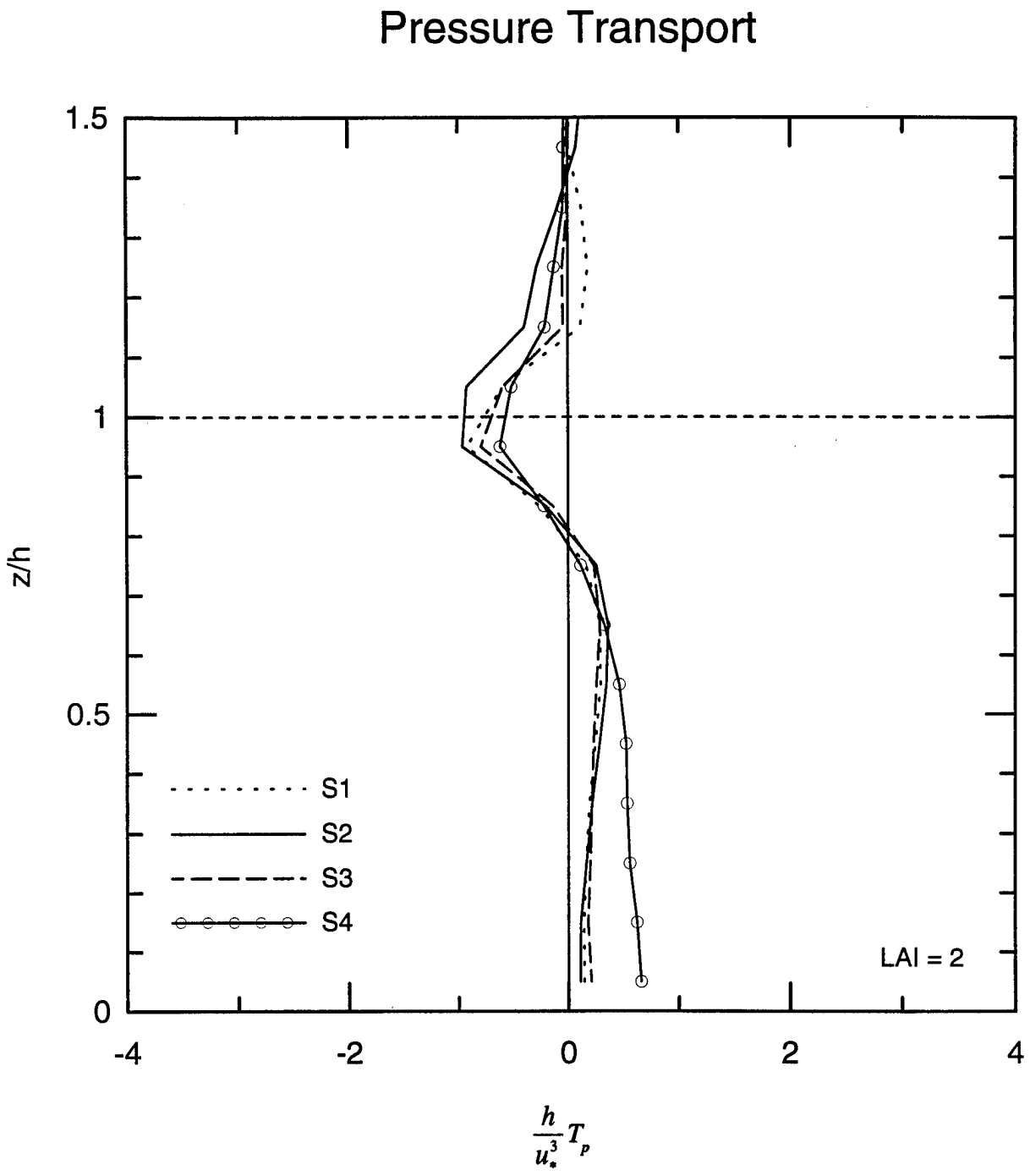

Figure 9a. Normalized pressure transport (T_p) for a sparse canopy LAI = 2. Plot labels are ordered in terms of increasingly negative h/L; S1 ($h/L = -0.024$), S2 (-0.074), S3 (-0.185), S4 (-1.398).

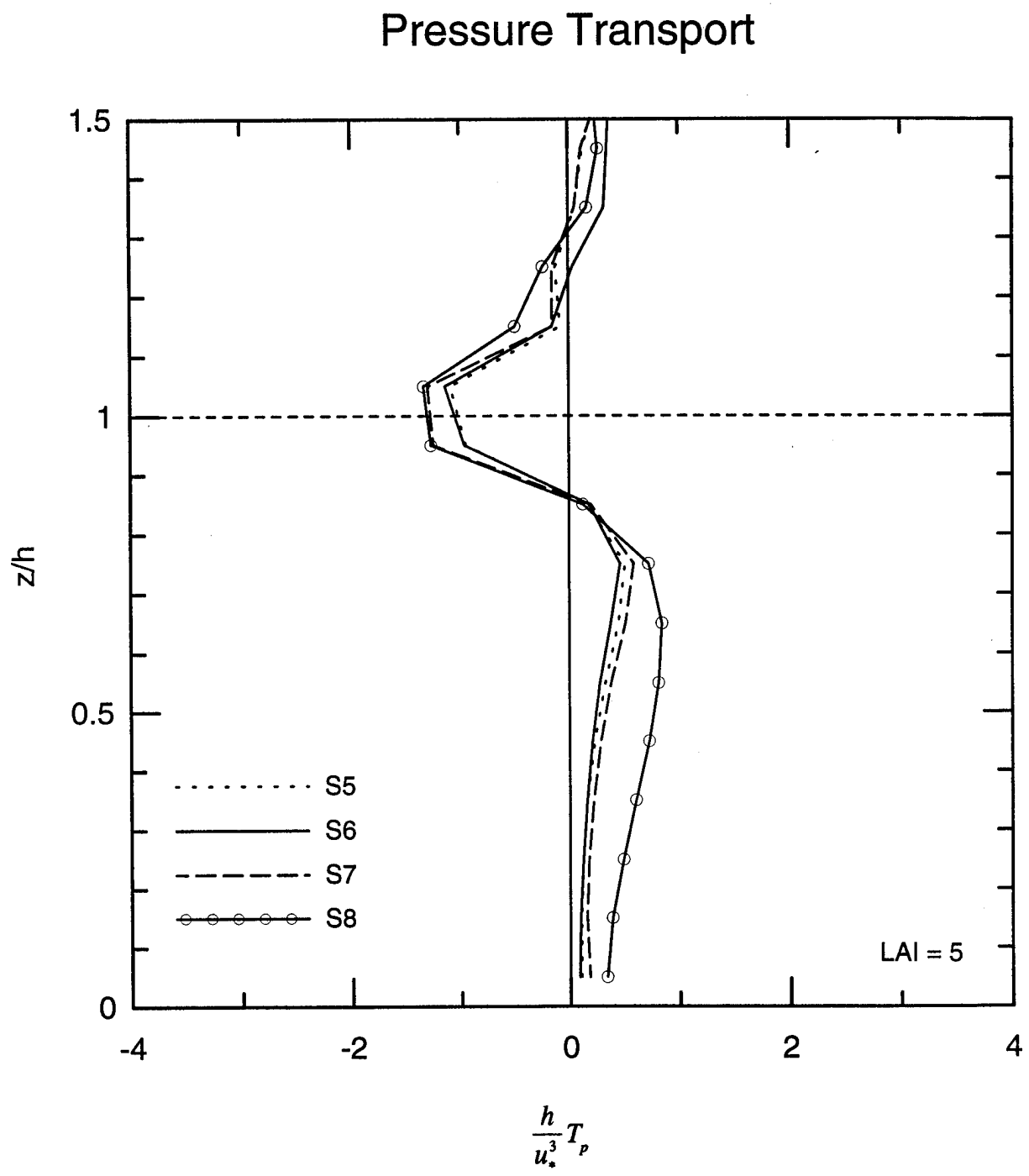

Figure 9b. Normalized pressure transport (T_p) for a dense canopy LAI = 5. Plot labels are ordered in terms of increasingly negative h/L; S5($h/L = -0.017$), S6(-0.064), S7(-0.153), S8(-1.252).

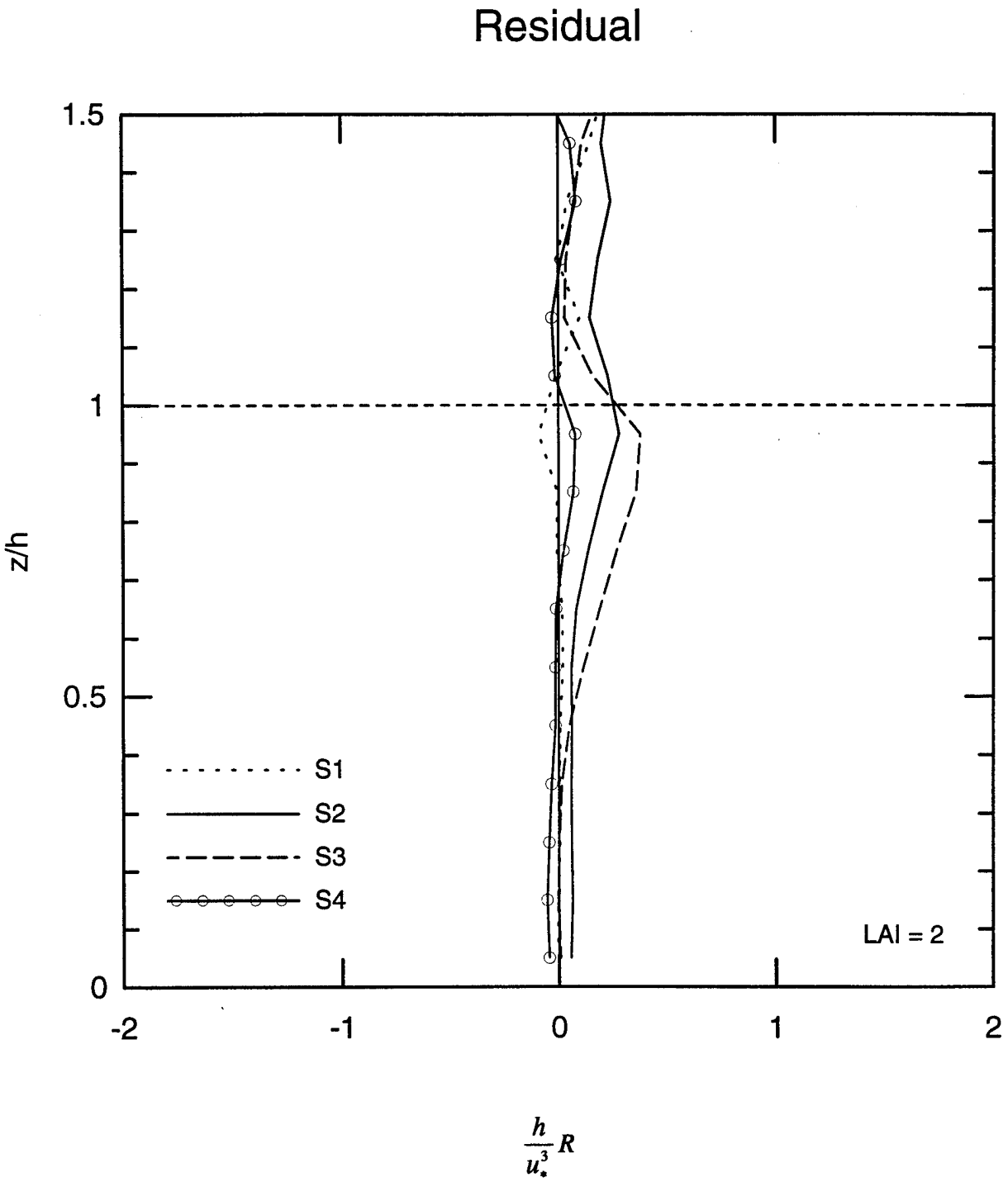

Figure 10a. Normalized residual (R) for a sparse canopy LAI = 2. Plot labels are ordered in terms of increasingly negative h/L ; S1 ($h/L = -0.024$), S2 (-0.074), S3 (-0.185), S4 (-1.398).

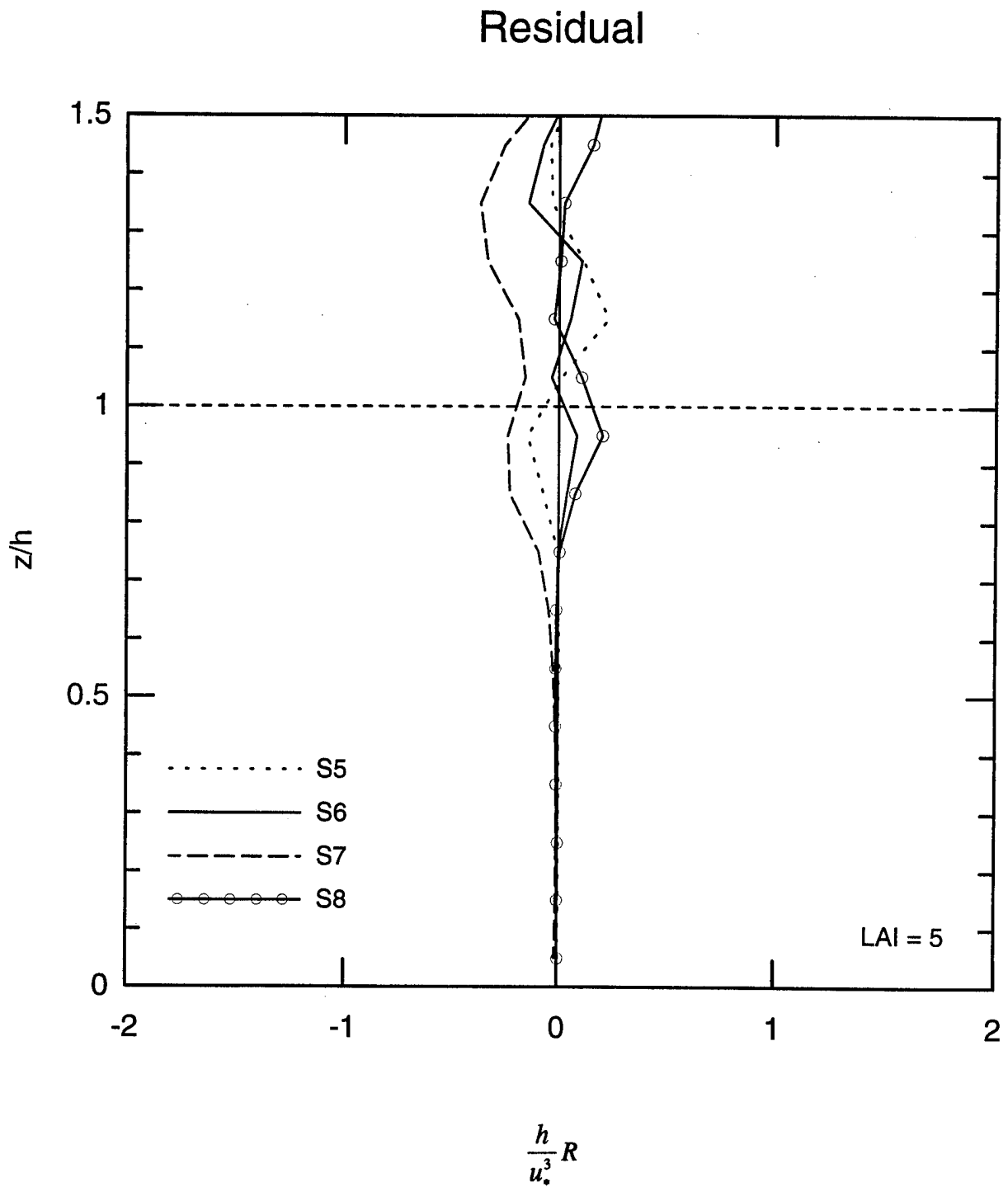

Figure 10b. Normalized residual (R) for a dense canopy LAI = 5. Plot labels are ordered in terms of increasingly negative h/L; S5(h/L=–0.017), S6(–0.064), S7(–0.153), S8(–1.252).

Appendix A

Derivation of the resolved scale momentum equation

The resolved scale momentum equation was derived from the Navier-Stokes equation for an incompressible, Boussinesq fluid. In tensor notation the momentum equation is

$$\frac{\partial u_i}{\partial t} = -\frac{\partial u_i u_j}{\partial x_j} - \frac{1}{\rho}\frac{\partial p}{\partial x_i} + \frac{g}{\theta_\circ}\theta\delta_{i3} + \nu\frac{\partial^2 u_i}{\partial x_j \partial x_j} \tag{A1}$$

In LES the resolved scale part of the flow is numerically defined by applying a filter function to the governing equations. Filtering the Navier-Stokes equation gives

$$\frac{\partial \overline{u}_i}{\partial t} = -\frac{\partial \overline{u_i u_j}}{\partial x_j} - \overline{\frac{1}{\rho}\frac{\partial p}{\partial x_i}} + \frac{g}{\theta_\circ}\overline{\theta}\delta_{i3} + \nu\overline{\frac{\partial^2 u_i}{\partial x_j \partial x_j}} \tag{A2}$$

where the overbar represents the filter process. The velocity components in the advection term must be partitioned into a resolved scale part and a subgrid scale part, $u_i = \overline{u}_i + u_i'$, to avoid writing an equation for $\overline{u_i u_j}$ (Leonard, 1974). In addition, the presence of the plant canopy complicates the filtering process. The horizontal pressure differentiation and the Laplacian should not commute with the filtering due to discontinuities across the plant elements according to arguments concerning horizontal averaging and differentiation presented in Wilson and Shaw (1977) and Raupach and Shaw (1982). Therefore, the pressure was also partitioned into a resolved scale part and a subgrid scale part, and performing the substitution gives

$$\frac{\partial \overline{u}_i}{\partial t} = -\frac{\partial \overline{\overline{u}_i \overline{u}_j}}{\partial x_j} - \frac{\partial \overline{\left(u_i' \overline{u}_j + \overline{u}_i u_j' + u_i' u_j'\right)}}{\partial x_j} - \frac{1}{\rho}\frac{\partial \overline{\overline{p}}}{\partial x_i} - \overline{\frac{1}{\rho}\frac{\partial p'}{\partial x_i}}$$

$$+\frac{g}{\theta_\circ}\overline{\theta}\delta_{i3} + \nu\frac{\partial^2 \overline{\overline{u}_i}}{\partial x_j \partial x_j} + \nu\overline{\frac{\partial^2 u_i'}{\partial x_j \partial x_j}} \qquad \text{(A3)}$$

where the second term on the right hand side represents the energy transfer between the resolved and the subgrid scales. The fourth and seventh terms represent form and viscous drag across the plant elements, respectively (Wilson and Shaw, 1977; Raupach and Shaw, 1982). Both effects were parameterized as one term, and for ease of presentation the viscous drag term will not be carried through in the derivation. In addition, the effects of molecular diffusion are negligible on the resolved scale and are not retained.

The filtering process is different from the traditional statistical averaging for turbulent flow. In general,

$$\overline{f'} \neq 0 \quad \text{and} \quad \overline{\overline{f}} \neq \overline{f} \qquad \text{(A4)}$$

However, the inequalities in (A4) could be equated depending on the chosen filter (Reynolds, 1990). The filter used in the LES here was chosen such that the equalities hold; thus, (A3) becomes

$$\frac{\partial \overline{u}_i}{\partial t} = -\frac{\partial \overline{u}_i \overline{u}_j}{\partial x_j} - \frac{\partial \overline{u_i' u_j'}}{\partial x_j} - \frac{1}{\rho}\frac{\partial \overline{p}}{\partial x_i} + \frac{g}{\theta_\circ}\overline{\theta}\delta_{i3} - \overline{\frac{1}{\rho}\frac{\partial p'}{\partial x_i}} \qquad \text{(A5)}$$

Next, the advection term in current LES were written in rotational form to give

$$\frac{\partial \overline{u}_i}{\partial t} = -\overline{u}_j\left(\frac{\partial \overline{u}_i}{\partial x_j} - \frac{\partial \overline{u}_i}{\partial x_j}\right) - \frac{\partial}{\partial x_i}\left(\frac{\overline{u}_j\overline{u}_j}{2}\right) + \frac{g}{\theta_\circ}\overline{\theta}\delta_{i3}$$

$$-\frac{1}{\rho}\frac{\partial}{\partial x_i}\left(\frac{\overline{p}''}{\rho} + \frac{R_{kk}}{3}\right) - \frac{1}{\rho}\frac{\partial\langle\overline{p}\rangle}{\partial x_i} - \frac{\partial \tau_{ij}}{\partial x_j} - \overline{\frac{1}{\rho}\frac{\partial p'}{\partial x_i}} \qquad \text{(A6)}$$

where

$$\tau_{ij} = R_{ij} - R_{kk}\frac{\delta_{ij}}{3} \qquad \text{(A7)}$$

$$R_{ij} = \overline{u_i'u_j'} \qquad \text{(A8)}$$

Equation (A7) represents the subgrid scale shear stresses, where the normal components were subtracted, and an equal and opposite term was added to the resolved scale pressure (A6). In addition, the horizontal mean pressure (angled brackets) gradient was separated from the resolved scale pressure and treated as an external forcing. As a result of the separation, the pressure in the fourth term on the right hand side represents the deviation from the horizontal mean indicated by the double primes. The resolved scale momentum equation that was used to form the turbulent kinetic energy budget is

$$\frac{\partial \overline{u}_i}{\partial t} = -\overline{u}_j\left(\frac{\partial \overline{u}_i}{\partial x_j} - \frac{\partial \overline{u}_i}{\partial x_j}\right) - \frac{\partial}{\partial x_i}\left(\frac{\overline{u}_j\overline{u}_j}{2}\right) - \frac{2}{3}\frac{\partial \overline{e'}}{\partial x_i} + \frac{g}{\theta_\circ}\overline{\theta}\delta_{i3}$$

$$-\frac{1}{\rho}\frac{\partial}{\partial x_i}\left(\frac{\overline{p}''}{\rho}\right) - \frac{1}{\rho}\frac{\partial\langle\overline{p}\rangle}{\partial x_i} - \frac{\partial \tau_{ij}}{\partial x_j} - \overline{\frac{1}{\rho}\frac{\partial p'}{\partial x_i}} \qquad \text{(A9)}$$

where $\overline{e'} \equiv \overline{u_i'u_i'}/2$ is the subgrid scale kinetic energy.

Finally, two parameterizations were used in (A9). The subgrid scale shear stress was represented in terms of the resolved scale strain rate of the form

$$\tau_{ij} = -K_M\left(\frac{\partial \bar{u}_i}{\partial x_j} + \frac{\partial \bar{u}_j}{\partial x_i}\right) \tag{A10}$$

where the diffusion coefficient was represented as a function of the subgrid scale kinetic energy and a dissipation length (Moeng, 1984).

The canopy drag effects were parameterized as

$$\overline{\frac{1}{\rho}\frac{\partial p'}{\partial x_i}} = C_d a(z) V \bar{u}_i \tag{A11}$$

where C_d is the isotropic drag coefficient; $a(z)$ is the leaf area density; and V is the vector magnitude wind.

Appendix B

Derivation of the horizontal mean momentum equation

The horizontal mean momentum equation was derived from the resolved scale momentum equation (A9) in the following manner: first the flow variables were portioned into a horizontal mean and a deviation therefrom; such as, $\overline{u}_i = \langle \overline{u}_i \rangle + \overline{u}_i''$; and a horizontal average was then performed to give the horizontal mean momentum equation. A term by term derivation follows:

The left hand side of (A9) is

$$\left\langle \frac{\partial \overline{u}_i}{\partial t} \right\rangle = \left\langle \frac{\partial \langle \overline{u}_i \rangle + \overline{u}_i''}{\partial t} \right\rangle = \left\langle \frac{\partial \langle \overline{u}_i \rangle}{\partial t} \right\rangle + \left\langle \frac{\partial \overline{u}_i''}{\partial t} \right\rangle = \frac{\partial \langle \overline{u}_i \rangle}{\partial t} + \frac{\partial \langle \overline{u}_i'' \rangle}{\partial t} = \frac{\partial \langle \overline{u}_i \rangle}{\partial t} \qquad \text{(B1)}$$

where the time differentiation and horizontal average commute provided the plant parts are not waving (Raupach and Shaw, 1982), $\langle \overline{u}_i'' \rangle = 0$ by definition. On the right hand side of (A9) the expansion of the rotational part of the advection term is

$$\begin{aligned}
\left\langle -\overline{u}_j \left(\frac{\partial \overline{u}_i}{\partial x_j} - \frac{\partial \overline{u}_j}{\partial x_i} \right) \right\rangle &= - \left\langle \left(\langle \overline{u}_j \rangle + \overline{u}_j'' \right) \left(\frac{\partial \left(\langle \overline{u}_i \rangle + \overline{u}_i'' \right)}{\partial x_j} - \frac{\partial \left(\langle \overline{u}_j \rangle + \overline{u}_j'' \right)}{\partial x_i} \right) \right\rangle \\
&= - \left\langle \langle \overline{u}_j \rangle \left(\frac{\partial \langle \overline{u}_i \rangle}{\partial x_j} - \frac{\partial \langle \overline{u}_j \rangle}{\partial x_i} \right) \right\rangle - \left\langle \langle \overline{u}_j \rangle \left(\frac{\partial \overline{u}_i''}{\partial x_j} - \frac{\partial \overline{u}_j''}{\partial x_i} \right) \right\rangle \\
&\quad - \left\langle \overline{u}_j'' \left(\frac{\partial \langle \overline{u}_i \rangle}{\partial x_j} - \frac{\partial \langle \overline{u}_j \rangle}{\partial x_i} \right) \right\rangle - \left\langle \overline{u}_j'' \left(\frac{\partial \overline{u}_i''}{\partial x_j} - \frac{\partial \overline{u}_j''}{\partial x_i} \right) \right\rangle \\
&= - \langle \overline{u}_j \rangle \left(\frac{\partial \langle \overline{u}_i \rangle}{\partial x_j} - \frac{\partial \langle \overline{u}_j \rangle}{\partial x_i} \right) - \left\langle \overline{u}_j'' \left(\frac{\partial \overline{u}_i''}{\partial x_j} - \frac{\partial \overline{u}_j''}{\partial x_i} \right) \right\rangle
\end{aligned} \qquad \text{(B2)}$$

The averaging process and horizontal differentiation commute in this case because the first-order spatial differentiation and horizontal averaging commute (Raupach and Shaw, 1982). As a result, the second and third term are zero on the horizontal average. Partitioning the kinetic energy part of the advection term gives

$$\begin{aligned}\left\langle -\frac{1}{2}\frac{\partial \overline{u}_j \overline{u}_j}{\partial x_i}\right\rangle &= -\left\langle \frac{1}{2}\frac{\partial\left(\langle \overline{u}_j\rangle + \overline{u}_j''\right)\left(\langle \overline{u}_j\rangle + \overline{u}_j''\right)}{\partial x_i}\right\rangle \\ &= -\left\langle \frac{1}{2}\frac{\partial \langle \overline{u}_j\rangle\langle \overline{u}_j\rangle}{\partial x_i}\right\rangle - \left\langle \frac{\partial \langle \overline{u}_j\rangle \overline{u}_j''}{\partial x_i}\right\rangle - \left\langle \frac{1}{2}\frac{\partial \overline{u}_j'' \overline{u}_j''}{\partial x_i}\right\rangle \\ &= -\frac{1}{2}\frac{\partial \langle \overline{u}_j\rangle\langle \overline{u}_j\rangle}{\partial x_i} - \left\langle \frac{1}{2}\frac{\partial \overline{u}_j'' \overline{u}_j''}{\partial x_i}\right\rangle\end{aligned} \tag{B3}$$

where the second term drops out on the horizontal average. The buoyancy term is

$$\left\langle \frac{g}{\theta_\circ}\overline{\theta}\delta_{i3}\right\rangle = \left\langle \frac{g}{\theta_\circ}\left(\langle \overline{\theta}\rangle + \overline{\theta}''\right)\delta_{i3}\right\rangle = \frac{g}{\theta_\circ}\langle \overline{\theta}\rangle\delta_{i3} \tag{B4}$$

The plant canopy effects, form drag, are parameterized in the model in the following manner

$$-\overline{\frac{1}{\rho}\frac{\partial p'}{\partial x_i}} = -C_d a(z) V \overline{u}_i \tag{B5}$$

and this is symbolically partitioned as

$$\left\langle -\overline{\frac{1}{\rho}\frac{\partial p'}{\partial x_i}}\right\rangle = \left\langle \left\langle -\overline{\frac{1}{\rho}\frac{\partial p'}{\partial x_i}}\right\rangle + \left(-\overline{\frac{1}{\rho}\frac{\partial p'}{\partial x_i}}\right)''\right\rangle = \left\langle -\overline{\frac{1}{\rho}\frac{\partial p'}{\partial x_i}}\right\rangle \tag{B6}$$

The SGS kinetic energy gradient is partitioned in a similar manner, and it equals

$$\left\langle -\frac{2}{3}\frac{\partial \overline{e'}}{\partial x_i}\right\rangle = \left\langle -\left\langle \frac{2}{3}\frac{\partial \overline{e'}}{\partial x_i}\right\rangle - \left(\frac{2}{3}\frac{\partial \overline{e'}}{\partial x_i}\right)''\right\rangle = -\left\langle \frac{2}{3}\frac{\partial \overline{e'}}{\partial x_i}\right\rangle \tag{B7}$$

Finally partitioning the SGS shear stresses and performing the horizontal average gives

$$\begin{aligned}
-\left\langle \frac{\partial \tau_{ij}}{\partial x_j}\right\rangle &= -\left\langle \frac{\partial}{\partial x_j}\left\{-K_M\left(\frac{\partial \overline{u}_i}{\partial x_j}+\frac{\partial \overline{u}_j}{\partial x_i}\right)\right\}\right\rangle \\
&= -\left\langle \frac{\partial}{\partial x_j}\left\{-\left(\langle K_M\rangle + K_M''\right)\left(\frac{\partial\left(\langle \overline{u}_i\rangle + \overline{u}_i''\right)}{\partial x_j}+\frac{\partial\left(\langle \overline{u}_j\rangle + \overline{u}_j''\right)}{\partial x_i}\right)\right\}\right\rangle \\
&= -\left\langle \frac{\partial}{\partial x_j}\left\{-\langle K_M\rangle\left(\frac{\partial \langle \overline{u}_i\rangle}{\partial x_j}+\frac{\partial \langle \overline{u}_j\rangle}{\partial x_i}\right)\right\}\right\rangle \\
&\quad -\left\langle \frac{\partial}{\partial x_j}\left\{-\langle K_M\rangle\left(\frac{\partial \overline{u}_i''}{\partial x_j}+\frac{\partial \overline{u}_j''}{\partial x_i}\right)\right\}\right\rangle \\
&\quad -\left\langle \frac{\partial}{\partial x_j}\left\{-K_M''\left(\frac{\partial \langle \overline{u}_i\rangle}{\partial x_j}+\frac{\partial \langle \overline{u}_j\rangle}{\partial x_i}\right)\right\}\right\rangle \\
&\quad -\left\langle \frac{\partial}{\partial x_j}\left\{-K_M''\left(\frac{\partial \overline{u}_i''}{\partial x_j}+\frac{\partial \overline{u}_j''}{\partial x_i}\right)\right\}\right\rangle
\end{aligned} \tag{B8}$$

The eddy diffusivity is a function of the SGS kinetic energy; thus, the horizontal averaging and differentiation should commute. Therefore, the second and third terms will equal zero, and the result is

$$\begin{aligned}
\left\langle -\frac{\partial \tau_{ij}}{\partial x_j}\right\rangle &= -\frac{\partial}{\partial x_j}\left\{-\langle K_M\rangle\left(\frac{\partial \langle \overline{u}_i\rangle}{\partial x_j}+\frac{\partial \langle \overline{u}_j\rangle}{\partial x_i}\right)\right\} \\
&\quad -\left\langle \frac{\partial}{\partial x_j}\left\{-K_M''\left(\frac{\partial \overline{u}_i''}{\partial x_j}+\frac{\partial \overline{u}_j''}{\partial x_i}\right)\right\}\right\rangle
\end{aligned} \tag{B9}$$

Finally, combining terms gives the resolved scale horizontal mean momentum

$$\underbrace{\frac{\partial\langle\bar{u}_i\rangle}{\partial t}}_{I} = \underbrace{-\langle\bar{u}_j\rangle\left(\frac{\partial\langle\bar{u}_i\rangle}{\partial x_j}-\frac{\partial\langle\bar{u}_j\rangle}{\partial x_i}\right)-\frac{1}{2}\frac{\partial\langle\bar{u}_j\rangle\langle\bar{u}_j\rangle}{\partial x_i}}_{II} \underbrace{-\left\langle\bar{u}_j''\left(\frac{\partial\bar{u}_i''}{\partial x_j}-\frac{\partial\bar{u}_j''}{\partial x_i}\right)\right\rangle}_{III}$$
$$\underbrace{-\left\langle\frac{1}{2}\frac{\partial\bar{u}_j''\bar{u}_j''}{\partial x_i}\right\rangle}_{III}+\underbrace{\frac{g}{\theta_\circ}\langle\bar{\theta}\rangle\delta_{i3}}_{IV}\underbrace{-\frac{\partial\langle\bar{p}\rangle}{\partial x}\delta_{i1}}_{V}\underbrace{-\left\langle\overline{\frac{1}{\rho}\frac{\partial p'}{\partial x_i}}\right\rangle}_{VI}\underbrace{-\left\langle\frac{2}{3}\frac{\partial\bar{e}'}{\partial x_i}\right\rangle}_{VII} \qquad \text{(B10)}$$
$$\underbrace{-\frac{\partial}{\partial x_j}\left\{-\langle K_M\rangle\left(\frac{\partial\langle\bar{u}_i\rangle}{\partial x_j}+\frac{\partial\langle\bar{u}_j\rangle}{\partial x_i}\right)\right\}-\left\langle\frac{\partial}{\partial x_j}\left\{-K_M''\left(\frac{\partial\bar{u}_i''}{\partial x_j}+\frac{\partial\bar{u}_j''}{\partial x_i}\right)\right\}\right\rangle}_{VIII}$$

where the terms represent

Term I: local time rate of change of horizontal mean momentum

Term II: advection of horizontal mean momentum by the mean wind

Term III: Reynolds stress terms

Term IV: buoyancy

Term V: mean pressure gradient

Term VI: form drag on the mean wind due to plant canopy-airflow interaction

Term VII: SGS normal stresses

Term VIII: parameterized SGS shear stresses

Appendix C

Derivation of the horizontal deviation momentum equation

The horizontal deviation momentum equation was derived in the conventional manner where the horizontal mean momentum equation (B10) was subtracted from the resolved scale momentum equation (A9). The flow variables in the resolved scale momentum equation were first partitioned into a horizontal mean and a deviation therefrom of the form:

$$\begin{aligned}
\frac{\partial\langle\overline{u}_i\rangle}{\partial t}+\frac{\partial\overline{u}_i''}{\partial t} = &-\langle\overline{u}_j\rangle\left(\frac{\partial\langle\overline{u}_i\rangle}{\partial x_j}-\frac{\partial\langle\overline{u}_j\rangle}{\partial x_i}\right)-\langle\overline{u}_j\rangle\left(\frac{\partial\overline{u}_i''}{\partial x_j}-\frac{\partial\overline{u}_j''}{\partial x_i}\right)\\
&-\overline{u}_j''\left(\frac{\partial\langle\overline{u}_i\rangle}{\partial x_j}-\frac{\partial\langle\overline{u}_j\rangle}{\partial x_i}\right)-\overline{u}_j''\left(\frac{\partial\overline{u}_i''}{\partial x_j}-\frac{\partial\overline{u}_j''}{\partial x_i}\right)-\frac{1}{2}\frac{\partial\langle\overline{u}_j\rangle\langle\overline{u}_j\rangle}{\partial x_i}\\
&-\frac{\partial\langle\overline{u}_j\rangle\overline{u}_j''}{\partial x_i}-\frac{1}{2}\frac{\partial\overline{u}_j''\overline{u}_j''}{\partial x_i}+\frac{g}{\theta_o}\left(\langle\overline{\theta}\rangle+\overline{\theta}''\right)\delta_{i3}-\frac{1}{\rho}\frac{\partial\overline{p}''}{\partial x_i}-\frac{\partial\langle\overline{p}\rangle}{\partial x_i}\\
&-\left\langle\overline{\frac{1}{\rho}\frac{\partial p'}{\partial x_i}}\right\rangle-\left(\overline{\frac{1}{\rho}\frac{\partial p'}{\partial x_i}}\right)''-\left\langle\frac{2}{3}\frac{\partial\overline{e'}}{\partial x_i}\right\rangle-\left(\frac{2}{3}\frac{\partial\overline{e'}}{\partial x_i}\right)''\\
&-\frac{\partial}{\partial x_j}\left\{-\langle K_M\rangle\left(\frac{\partial\langle\overline{u}_i\rangle}{\partial x_j}+\frac{\partial\langle\overline{u}_j\rangle}{\partial x_i}\right)\right\}-\frac{\partial}{\partial x_j}\left\{-\langle K_M\rangle\left(\frac{\partial\overline{u}_i''}{\partial x_j}+\frac{\partial\overline{u}_j''}{\partial x_i}\right)\right\}\\
&-\frac{\partial}{\partial x_j}\left\{-K_M''\left(\frac{\partial\langle\overline{u}_i\rangle}{\partial x_j}+\frac{\partial\langle\overline{u}_j\rangle}{\partial x_i}\right)\right\}-\frac{\partial}{\partial x_j}\left\{-K_M''\left(\frac{\partial\overline{u}_i''}{\partial x_j}+\frac{\partial\overline{u}_j''}{\partial x_i}\right)\right\}
\end{aligned}\qquad \text{(C1)}$$

and subtract the horizontal mean momentum equation giving

$$\frac{\partial \overline{u}_i''}{\partial t} = -\langle \overline{u}_j \rangle \left(\frac{\partial \overline{u}_i''}{\partial x_j} - \frac{\partial \overline{u}_j''}{\partial x_i} \right) - \overline{u}_j'' \left(\frac{\partial \langle \overline{u}_i \rangle}{\partial x_j} - \frac{\partial \langle \overline{u}_j \rangle}{\partial x_i} \right) - \overline{u}_j'' \left(\frac{\partial \overline{u}_i''}{\partial x_j} - \frac{\partial \overline{u}_j''}{\partial x_i} \right) -$$

$$- \frac{\partial \langle \overline{u}_j \rangle \overline{u}_j''}{\partial x_i} - \frac{1}{2} \frac{\partial \overline{u}_j'' \overline{u}_j''}{\partial x_i} + \frac{g}{\theta_\circ} \overline{\theta}'' \delta_{i3} - \frac{1}{\rho} \frac{\partial \overline{p}''}{\partial x_i} - \left(\overline{\frac{1}{\rho} \frac{\partial p'}{\partial x_i}} \right)'' - \left(\frac{2}{3} \frac{\partial \overline{e'}}{\partial x_i} \right)''$$

$$- \frac{\partial}{\partial x_j} \left\{ -\langle K_M \rangle \left(\frac{\partial \overline{u}_i''}{\partial x_j} + \frac{\partial \overline{u}_j''}{\partial x_i} \right) \right\} - \frac{\partial}{\partial x_j} \left\{ -K_M'' \left(\frac{\partial \langle \overline{u}_i \rangle}{\partial x_j} + \frac{\partial \langle \overline{u}_j \rangle}{\partial x_i} \right) \right\} \qquad \text{(C2)}$$

$$- \frac{\partial}{\partial x_j} \left\{ -K_M'' \left(\frac{\partial \overline{u}_i''}{\partial x_j} + \frac{\partial \overline{u}_j''}{\partial x_i} \right) \right\}$$

$$+ \left\langle \overline{u}_j'' \left(\frac{\partial \overline{u}_i''}{\partial x_j} - \frac{\partial \overline{u}_j''}{\partial x_i} \right) \right\rangle + \left\langle \frac{1}{2} \frac{\partial \overline{u}_j'' \overline{u}_j''}{\partial x_i} \right\rangle + \left\langle \frac{\partial}{\partial x_j} \left\{ -K_M'' \left(\frac{\partial \overline{u}_i''}{\partial x_j} + \frac{\partial \overline{u}_j''}{\partial x_i} \right) \right\} \right\rangle$$

The advection terms can be simplified using the product rule, and equation (C2) can be written as

$$\underbrace{\frac{\partial \overline{u}_i''}{\partial t}}_{I} = \underbrace{-\langle \overline{u}_j \rangle \frac{\partial \overline{u}_i''}{\partial x_j}}_{II} \underbrace{- \overline{u}_j'' \frac{\partial \langle \overline{u}_i \rangle}{\partial x_j}}_{III} \underbrace{- \overline{u}_j'' \left(\frac{\partial \overline{u}_i''}{\partial x_j} - \frac{\partial \overline{u}_j''}{\partial x_i} \right) - \frac{1}{2} \frac{\partial \overline{u}_j'' \overline{u}_j''}{\partial x_i}}_{IV} + \underbrace{\left\langle \left(\frac{\partial \overline{u}_i'' \overline{u}_j''}{\partial x_j} \right) \right\rangle}_{V}$$

$$\underbrace{+ \frac{g}{\theta_\circ} \overline{\theta}'' \delta_{i3}}_{VI} \underbrace{- \frac{1}{\rho} \frac{\partial \overline{p}''}{\partial x_i}}_{VII} \underbrace{- \left(\overline{\frac{1}{\rho} \frac{\partial p'}{\partial x_i}} \right)''}_{VIII} \underbrace{- \frac{2}{3} \frac{\partial \left(\overline{e'} \right)''}{\partial x_i}}_{IX} \qquad \text{(C3)}$$

$$\underbrace{- \frac{\partial \left(\tau_{ij} \right)''}{\partial x_j} + \left\langle \frac{\partial}{\partial x_j} \left\{ -K_M'' \left(\frac{\partial \overline{u}_i''}{\partial x_j} + \frac{\partial \overline{u}_j''}{\partial x_i} \right) \right\} \right\rangle}_{X}$$

where the SGS stresses are defined as

$$-\frac{\partial\left(\tau_{ij}\right)''}{\partial x_j}=-\frac{\partial}{\partial x_j}\left\{-\langle K_M\rangle\left(\frac{\partial \overline{u}_i''}{\partial x_j}+\frac{\partial \overline{u}_j''}{\partial x_i}\right)\right\}-\frac{\partial}{\partial x_j}\left\{-K_M''\left(\frac{\partial\langle \overline{u}_i\rangle}{\partial x_j}+\frac{\partial\langle \overline{u}_j\rangle}{\partial x_i}\right)\right\}$$

$$-\frac{\partial}{\partial x_j}\left\{-K_M''\left(\frac{\partial \overline{u}_i''}{\partial x_j}+\frac{\partial \overline{u}_j''}{\partial x_i}\right)\right\}$$

The terms of (C3) represent

Term I: local time rate of change of deviation velocity component

Term II: advection of the deviation velocity by the mean wind

Term III: mean shear term

Term IV: advection of the deviation velocity by deviation velocity

Term V: Reynolds stress term

Term VI: buoyancy

Term VII: deviation pressure gradient

Term VIII: plant canopy drag effects

Term IX: SGS normal stresses

Term X: parameterized SGS shear stress

Appendix D

Derivation of the resolved scale turbulent kinetic energy equation

The resolved scale TKE equation for canopy flow was derived by multiplying the horizontal deviation momentum equation (C3) by a horizontal deviation velocity component, $\overline{u}_i''$, and then performing a horizontal average. The result is:

$$\frac{\partial\langle\overline{u}_i''\overline{u}_i''/2\rangle}{\partial t} = -\langle\overline{u}_i''\overline{u}_j''\rangle\frac{\partial\langle\overline{u}_i\rangle}{\partial x_j} + \frac{g}{\theta}\langle\overline{u}_i''\theta''\rangle\delta_{i3}$$
$$-\left\langle\overline{u}_i''\left\{\overline{u}_j''\left(\frac{\partial\overline{u}_i''}{\partial x_j} - \frac{\partial\overline{u}_j''}{\partial x_i}\right) + \frac{\partial\,\overline{u}_j''\overline{u}_j''/2}{\partial x_i}\right\}\right\rangle - \left\langle\frac{1}{\rho}\frac{\partial\overline{u}_i''\overline{p}''}{\partial x_i}\right\rangle \qquad \text{(D1)}$$
$$-\left\langle\overline{u}_i''\left(\overline{\frac{1}{\rho}\frac{\partial p'}{\partial x_i}}\right)''\right\rangle - \left\langle\overline{u}_i''\frac{2}{3}\frac{\partial\left(\overline{e'}\right)''}{\partial x_i} + \overline{u}_i''\frac{\partial\left(\tau_{ij}\right)''}{\partial x_j}\right\rangle$$

For steady, horizontally homogeneous conditions with negligible mean subsidence, the TKE budget becomes

$$\frac{\partial\langle\overline{E}''\rangle}{\partial t} = 0 = \underbrace{-\langle\overline{u}''\,\overline{w}''\rangle\frac{\partial\langle\overline{u}\rangle}{\partial z}}_{P_s} + \underbrace{\frac{g}{\theta}\langle\overline{w}''\,\theta''\rangle}_{P_b}$$
$$\underbrace{-\left\langle\frac{\partial\overline{w}''\,\overline{E}''}{\partial z}\right\rangle}_{T_t} \underbrace{-\left\langle\frac{1}{\rho}\frac{\partial\overline{w}''\,\overline{p}''}{\partial z}\right\rangle}_{T_p} + \underbrace{\left\langle\overline{u}_i''\,F_i''\right\rangle}_{D_{cd}}$$
$$\underbrace{-\left\langle\frac{2}{3}\frac{\partial\,\overline{u}_i''\left(\overline{e'}\right)''}{\partial x_i} + \frac{\partial\,\overline{u}_i''\left(\tau_{ij}\right)''}{\partial x_j} - \left(\tau_{ij}\right)''\frac{\partial\,\overline{u}_i''}{\partial x_j}\right\rangle}_{D_{sgs}} \qquad \text{(D2)}$$

where $\overline{E}'' = \overline{u}_i''\overline{u}_i''/2$ is the resolved scale turbulent kinetic energy, and the terms represent the following: P_s is the mean shear production; P_b is the buoyant production; T_t is the turbulent transport; T_p is the pressure transport; D_{cd} is the parameterized influence of plant canopy drag; and D_{sgs} represents the combined effects of subgrid scale diffusion of resolved scale TKE (first two terms) and the transfer of resolved scale TKE to the subgrid scales (last term).

References

Brost, R.A., J.C. Wyngaard, and D.H. Lenschow, 1982: Marine stratocumulus layers. Part II: Turbulence budgets. *J. Atmos. Sci.*, **39**, 818-836.

Brunet, Y., J.J. Finnigan and M.R. Raupach, 1994: A wind tunnel study of air flow in waving wheat: single-point velocity statistics. *Boundary-Layer Meteorol.*, **70**, 95-132.

Caughey, S.J. and J.C. Wyngaard, 1979: The turbulence kinetic energy budget in convective conditions. *Q. J. R. Meteorol. Soc.*, **105**, 231-239.

Deardorff, J.W, 1973: Three-dimensional numerical modeling of the planetary boundary layer, *Workshop in Micrometeorology*, D.A. Haguen (ed.), Amer. Meteor. Soc., Boston, 271-311.

Deardorff, J.W, 1980: Stratocumulus-capped mixed layers derived from a three-dimensional model. *Boundary-Layer Meteorol.*, **18**, 495-527.

Deardorff, J.W. and G.E. Willis, 1985: Further results from a laboratory model of the convective planetary layer. *Boundary-Layer Meteorol.*, **32**, 205-236.

Fox, D.G. and S.A. Orzag, 1973: Pseudospectral approximation to two-dimensional turbulence. *J. Comput. Phys.*, **11**, 612-619.

Gao, W., R.H. Shaw, and K.T. Paw U, 1989: Observation of organized structure in turbulent flow within and above a forest canopy. *Boundary-Layer Meteorol.*, **47**, 349-377.

Kaimal, and J.J. Finnigan, 1994: *Atmospheric Boundary Layer Flows: Their Structure and Measurement*, Oxford University Press, New York, pp. 81-83.

Kanda, M. and M. Hino, 1994: Organized structures in developing turbulent flow within and above a plant canopy, using a large eddy simulation. *Boundary-Layer Meteorol.*, **68**, 237-257.

LeClerc, M.Y., K.C. Beissner, R.H. Shaw, G. den Hartog, and H.H. Neumann, 1990: The influence of atmospheric stability on the budgets of the reynolds stress and turbulent kinetic energy budget within and above a deciduous forest. *J. Appl. Meteorol.*, **29**, 916-933.

Leonard, A., 1974: Energy cascade in large eddy simulations of turbulent fluid flow. *Advances in Geophysics.*, **18**, Academic Press, 237-248.

Lesnik, G.E., 1974: Results of measurement of turbulent energy balance components in a layer of vegetation. *Izv. Atmos. Oceanic Phys.*, **10**, 652-655.

Lenschow, D.H., J.C. Wyngaard, and W.T. Pennell, 1980: Mean-field and second moment budgets in a baroclinic, convective boundary layer. *J. Atmos. Sci.*, **37**, 1313-1326.

Maitani, T. and T. Seo, 1985: Estimates of velocity-pressure and velocity-pressure gradient interactions in the surface layer over plant canopies. *Boundary-Layer Meteorol.*, **33**, 51-60.

Mason, P. J., 1994: Large-eddy simulation: A critical review of the technique. *Q. J. R. Meteorol. Soc.*, **120**, 1-26.

Mason, P. J., 1989: Large-eddy simulation of the convective boundary layer. *J. Atmos. Sci.*, **46**, 1492-1516.

McBean, G.A. and J.A. Elliott, 1975: The vertical transports of kinetic energy and pressure in the boundary layer. *J. Atmos. Sci.*, **32**, 753-766.

Meyers, T.P. and K.T. Paw U, 1986: Testing of a higher-order closure model for flow within and above plant canopies. *Boundary-Layer Meteorol.*, **37**, 297-311.

Meyers, T.P. and K.T. Paw U, 1987: Modeling the plant canopy micrometeorology with higher-order closure principles. *Agric. For. Meteorol.*, **41**, 143-163.

Meyers, T.P. and D.D. Baldocchi, 1991: The budgets of turbulent kinetic energy and Reynolds stress within and above a deciduous forest. *Agric. For. Meteorol.*, **53**, 207-222.

Moeng, C.-H., 1984: A large-eddy simulation model for the study of planetary boundary-layer turbulence. *J. Atmos. Sci.*, **41**, 2052-2062.

Moeng, C.-H. and J. C. Wyngaard, 1988: Spectral analysis of large-eddy simulations of the convective boundary-layer. *J. Atmos. Sci.*, **45**, 3573-3587.

Moeng, C.-H. and J. C. Wyngaard, 1989: Evaluation of turbulent transport and dissipation closures in second-order modeling. *J. Atmos. Sci.*, **46**, 2311-2333.

Moeng, C.-H. and P. Sullivan, 1994: A comparison of shear and buoyant driven planetary boundary layer flows. *J. Atmos. Sci.*, **51**, 999-1022.

Nieuwstadt, F.T.M., P.J. Mason, C.-H. Moeng, and U. Schumann, 1993: Large-eddy simulation of the convective boundary layer: A comparison of four computer codes. *Turbulent Shear Flows 8*, Durst et al., Eds., Springer-Verlag, 431 pp.

Patton, E.G., R.H. Shaw, K.T. Paw U and C-H. Moeng, 1994: A Comparison of Two Large-Eddy Simulations of Turbulent Flow Above and Within a Forest Canopy. *Proc. 21st AMS Conference on Agricultural and Forest Meteorol.*, Amer. Meteor. Soc., Boston, 88-91.

Raupach, M.R. R.H. and Shaw, 1982: Averaging procedures for flow within vegetation canopies. *Boundary-Layer Meteorol.*, **22**, 79-90.

Raupach, M.R., P.A. Coppin, and B.J. Legg, 1986: Experiments on scalar dispersion within a model plant canopy, Part I: the turbulent structure. *Boundary-Layer Meteorol.*, **35**, 21-52.

Rayment, R. and S.J. Caughey, 1977: An investigation of the turbulence balance equations in the atmospheric boundary layer. *Boundary-Layer Meteorol.*, **11**, 15-26.

Reynolds, C.W., 1990: The potential and limitations of direct and large eddy simulations. *Lecture Notes in Physics.*, **357**, 313-343.

Shaw, R.H., G. den Hartog, and H.H. Neumann, 1988: Influence of foliar density and thermal stability on profiles of Reynolds stress and turbulence intensity in a deciduous forest. *Boundary-Layer Meteorol.*, **45**, 391-409.

Shaw, R.H., K.T. Paw U, X.J. Zhang, W. Gao, G. den Hartog, and H.H. Neumann, 1990: Retrieval of turbulent pressure fluctuations at the ground surface beneath a forest. *Boundary-Layer Meteorol.*, **50**, 319-338.

Shaw, R.H. and X.J. Zhang, 1992: Evidence of pressure-forced flow in a forest. *Boundary-Layer Meteorol.*, **58**, 273-288.

Shaw, R.H. and U. Schumann, 1992: Large-eddy simulation of turbulent flow above and within a forest. *Boundary-Layer Meteorol.*, **61**, 47-64.

Shaw, R.H. and I. Seginer, 1985: The dissipation of turbulence in plant canopies. *Proc., Seventh Symp. on Turbulence and Diffusion*, Amer. Meteor. Soc., Boston, 200-203.

Shi, G., R.H. Shaw, G.W. Thurtell, G. den Hartog, and H.H. Neumann, 1987: The turbulent kinetic energy budget within and above a deciduous forest. *Preprints, 18th Conference Agricultural and Forest Meteorology*, Amer. Meteor. Soc., Boston, 187-188.

Wilczak, J.M. and J.A. Businger, 1984: Large-scale eddies in the unstably stratified atmospheric surface layer. Part II: Turbulent pressure fluctuations and the budget of heat flux, stress and turbulent kinetic energy. *J. Atmos. Sci.*, **41**, 3551-3567.

Wilson, J.D., 1988: A second-order closure model for flow through vegetation, *Boundary-Layer Meteorol.*, **42**, 371-392.

Wilson, N.R. and R.H. Shaw, 1977: A higher order closure model fro canopy flow. *J. Appl. Meteorol.*, **16**, 1197-1205.

Wyngaard, J.C. and O.R. Coté, 1971: The budgets of turbulent kinetic energy and temperature variance in the atmospheric surface layer. *J. Atmos. Sci.*, **28**, 190-201.

Zeman, O. and J.L. Lumley, 1976: Modeling buoyancy driven mixed layers. *J. Atmos. Sci.*, **33**, 1974-1988.

Zhuang, Y. and B. D. Amiro, 1994: Pressure fluctuations during coherent motions and their effects on the budgets of turbulent kinetic energy and momentum flux within a forest canopy. *J. Appl. Meteorol.*, **33**, 704-711.